Two dynamical behaviours of the microtubules at cell cortex reveal pulling and pushing forces that position the spindle in *C. elegans* embryo.

H. Bouvrais[1,], L. Chesneau[1], D. Fairbrass[1], Y. Le Cunff[1], N. Soler[1], T. Pécot[2], C. Kervrann[2], J. Pécréaux[1]

[1]IGDR - CNRS UMR 6290, Université Rennes 1, Faculté de Médecine, 2 avenue du Professeur Léon Bernard, CS 34317, 35043 Rennes Cedex, France

[2]INRIA Rennes – Bretagne Atlantique, Campus Universitaire de Beaulieu, 35042 Rennes Cedex, France

Email: [helene.bouvrais@univ-rennes1.fr; jacques.pecreaux@univ-rennes1.fr]

14th May 2019

ABSTRACT

In the *Caenorhabditis elegans* zygote, astral microtubules generate forces, pushing against and pulling from the cell periphery. They are essential to position the mitotic spindle and in turn the cytokinesis furrow, ensuring the proper distribution of fate determinants to the daughter cells. By measuring the dynamics of astral microtubules, we revealed the presence of two populations, residing at the cortex during 0.4 s and 1.8 s, proposed to reflect the pulling and pushing events, respectively. This is a unique opportunity to unravel the time and space variations of these both spindle-positioning forces, to study their regulation under physiological conditions. By an investigation at the microscopic level, we first confirmed that the asymmetry in pulling forces was encoded by an anteroposterior imbalance in dynein-engaging rate, and that this asymmetry exists from early metaphase on and accounts for the final spindle position. More importantly, we obtained direct proof of the temporal control of pulling forces through the force-generator processivity increase during anaphase. Lastly, we discovered an anti-correlation between the long-lived population density and the stability of the spindle position during metaphase, which strongly suggests that the pushing forces contribute to maintaining the spindle at the cell centre.

KEYWORDS

Microtubule dynamics, single microtubule-mediated event, spindle positioning, mechanical forces, force-generator processivity regulation, polarity encoding, force coordination, multi-scale (molecular and cellular) approach.

INTRODUCTION

During asymmetric divisions, the position of the mitotic spindle is precisely regulated to correctly partition cell fate determinants, which is crucial to ensure faithful divisions during developmental processes (Gönczy, 2008; Neumüller and Knoblich, 2009; Morin and Bellaïche, 2011; McNally, 2013). In the one-cell embryo of the nematode *Caenorhabditis elegans*, the mitotic spindle is first oriented along the polarity axis and positioned at the cell centre. Then, the spindle is precisely maintained at that position for a few minutes during metaphase. Finally, it is displaced out of the cell centre prior to division (Gönczy, 2008; McNally, 2013). So far, cell-scale investigations revealed some forces at the core of this precise choreography, in particular, the pulling on astral microtubules from the cell cortex accounting for the posterior displacement of the spindle starting from mid metaphase. The force generators are composed of the dynein/dynactin complex, the LIN-5^{NuMA} protein, and the G-protein regulators GPR-1/2^{LGN}, and are anchored at the membrane through Gα subunits (Gotta and Ahringer, 2001; Colombo *et al.*, 2003; Srinivasan *et al.*, 2003; Couwenbergs *et al.*, 2007; Nguyen-Ngoc *et al.*, 2007). These force generators contribute by molecular motor action and by coupling with the microtubule depolymerisation (Schmidt *et al.*, 2005; Kozlowski *et al.*, 2007; Nguyen-Ngoc *et al.*, 2007; O'Rourke *et al.*, 2010; Laan *et al.*, 2012a). Balancing this cortical pulling, the centring force which maintains the spindle at the cell centre during metaphase is still under debate (Reinsch and Gonczy, 1998; Wühr *et al.*, 2009; Zhu *et al.*, 2010; Kimura and Kimura, 2011a; McNally, 2013; Wu *et al.*, 2017), with three possible forces implicated: the cortical pulling forces (Grill and Hyman, 2005; Kimura and Onami, 2005); the cytoplasmic pulling forces (Kimura and Kimura, 2011a; Shinar *et al.*, 2011; Barbosa *et al.*, 2017); and the cortical pushing forces (Pecreaux *et al.*, 2006a; Garzon-Coral *et al.*, 2016). So far, these studies were all based on cell-scale measures.

How these two mechanical forces, previously studied separately and spatially or temporally averaged, are regulated and coordinated in space and throughout mitosis? The cortical pulling forces are asymmetric, because of a higher number of active force generators – trimeric complexes engaged in pulling events with astral microtubules – at the posterior-most side of the embryo (Gotta *et al.*, 2003; Grill *et al.*, 2003; Pecreaux *et al.*, 2006a; Nguyen-Ngoc *et al.*, 2007), in response to polarity cues (Grill *et al.*, 2001; Colombo *et al.*, 2003; Tsou *et al.*, 2003a; Park and Rose, 2008; Bouvrais *et al.*, 2018). On top of that, the physical ground of the progressive increase in the pulling forces along the course of the division, was inferred from cell scale measurements (Labbe *et al.*, 2004; Pecreaux *et al.*, 2006a; Campbell *et al.*, 2009; Bouvrais *et al.*, 2018), and a molecular mechanism is still missing. Finally, little is known on the spatiotemporal regulation of the centring forces.

Astral microtubules are involved in generating all these forces. These semi-flexible filaments emanate from the spindle poles. They are dynamic, switching alternatively from growing to shrinking and back, at the catastrophe and rescue rates, respectively (Mitchison and Kirschner, 1984). At the cortex, astral microtubules can be in three different states: shrinking and pulling from there through minus-end directed dynein

molecules anchored at the cortex, which coordinate their motor action with microtubule shrinkage (Gonczy *et al.*, 1999; Dujardin and Vallee, 2002; Grishchuk *et al.*, 2005; Gusnowski and Srayko, 2011; Laan *et al.*, 2012a; Rodriguez-Garcia *et al.*, 2018); pushing and growing against the cortex (Faivre-Moskalenko and Dogterom, 2002; Dogterom *et al.*, 2005; Howard, 2006), helped by stabilizing associated proteins like CLASP (Espiritu *et al.*, 2012); or stalled, with microtubules being clamped at the cortex, neither growing or shrinking, possibly through dynein tethering (Hendricks *et al.*, 2012; Laan *et al.*, 2012a; Laan *et al.*, 2012b) or stabilizing proteins (Labbé *et al.*, 2003; Sugioka *et al.*, 2018). These different states are revealed by the microtubule dynamics at the cortex, especially their residence times that reflect their catastrophe rates. Furthermore, *in vitro* and computational studies have shown that dynein tethering delayed microtubule catastrophe (Hendricks *et al.*, 2012; Laan *et al.*, 2012a), while larger pushing forces would advance it (Janson *et al.*, 2003). Consequently, at cell-scale, different residence times are expected for microtubules involved either in pulling forces during anaphase (Pecreaux *et al.*, 2006a) or in pushing forces during metaphase (Pécréaux *et al.*, 2016) in *C. elegans* embryo, revealing the cortical microtubule-mediated force generating events.

Previous studies focussing on the residence times of astral microtubules at the *C. elegans* embryo cortex revealed some spatial modulations. In particular, microtubules are suggested to be more dynamic (lower lifetime) at the posterior cortex compared to anterior cortex, although the reported residence times are strikingly different between distinct studies (Labbé *et al.*, 2003; Kozlowski *et al.*, 2007; Gerhold *et al.*, 2018; Sugioka and Bowerman, 2018; Sugioka *et al.*, 2018). Furthermore, these studies provide reduced indications about how the contact durations evolve throughout mitosis. This limitation is made more acute by the short duration of these contacts (a few frames), in low signal-to-noise ratio images. Recent developments in microscopy and image processing tools call for revisiting this problem (Chenouard *et al.*, 2014; Meiniel *et al.*, 2018).

Beyond imaging improvements, the statistical analysis of the microtubule-end tracks at the cortex could also be significantly refined in contrast to the classic fit with a mono-exponential distribution (Kozlowski *et al.*, 2007; Sugioka *et al.*, 2018). In particular, and to distinguish several co-existing dynamical behaviours, we here fitted the experimental distribution of the contact durations with a finite-mixture-of-exponential models and then used an objective criterion to choose which model best fits the data. Such an approach, although delicate, benefits of developments in applied mathematics (Grinvald and Steinberg, 1974; James and Ware, 1985; Vieland and Hodge, 1998; Jae Myung *et al.*, 2000; Turton *et al.*, 2003). The microtubule residence times could last only a few tenths of a second, corresponding to a few frames, calling for specific analysis as performed in photon counting experiments. This field has designed appropriate fitting strategies that offer a firm starting point to analyse microtubule dynamics (Maus *et al.*, 2001; Turton *et al.*, 2003; Nishimura and Tamura, 2005; Laurence and Chromy, 2010).

In the present paper, we aimed to study the spatiotemporal regulation of the spindle-positioning forces during the first division of the *C. elegans* embryo. To do so, the microtubule dynamics at the cortex were instrumental. We designed the DiLiPop assay

for "Distinct Lifetime subPopulation assay" to faithfully disentangle several microtubule populations, distinct by their dynamics at the cortex and found two of them, which we could associate with different microtubule functions. Equipped with this assay, we could for the first time resolve in time and space, and at the microscopic level, how the forces positioning the spindle are regulated during mitosis. In particular, first, we measured a force-generator processivity increase during anaphase revealing how pulling forces are regulated throughout mitosis; and, second, we identified which mechanism enables to maintain the spindle at cell centre during metaphase. Importantly, we also suggest how these forces coordinate in space and time.

RESULTS

The Distinct Lifetime (sub)Population assay reveals two populations of microtubules at the cortex.

To investigate the regulation of the forces exerted on the mitotic spindle during the first mitosis of the *C. elegans* zygote, we set to measure the dynamics of astral microtubules at the cortex. The microtubules were entirely fluorescently labelled using YFP::α-tubulin (Supp. Text §1.1.1), since we aimed to visualise the microtubules in all their force generating modalities, revealed by growing, shrinking or stalled states. We performed spinning disk microscopy at the cortical plane, at 10 frames per second similarly to (Bouvrais *et al.*, 2018) (Supp. Text §1.1.2). The microtubules contacting the cortex end-on, they appeared as spots during metaphase and anaphase (Movie S1) (Gusnowski and Srayko, 2011). The high frame rate, needed to resolve microtubule residing briefly at the cortex, led to images with a low signal-to-noise ratio (Figure 1A, top). We thus denoised them using the Kalman filter (Figure 1A, middle) (Kalman, 1960) before tracking the microtubule contacts using u-track algorithm (Figure 1A, bottom, Table S1, Supp. Text §1.1.3) (Jaqaman *et al.*, 2008). This image-processing pipeline is further named KUT.
We computed the duration distributions of the tracks for each embryo separately (to avoid averaging artefacts) (Figure 1B). When all the microtubules have the same catastrophe rate, this distribution follows an exponential decay (Kozlowski *et al.*, 2007; Floyd *et al.*, 2010). However, we also envisaged that multiple force-generating mechanisms involving microtubules are superimposed, corresponding to distinct catastrophe rates. Therefore, we fitted the distribution with finite-mixture-of-exponential models, in particular double- and triple- exponential models (Supp. Text §1.2.1). Double-exponential better fitted the duration-distribution suggesting that we observed at least two populations of microtubules at the cortex of *C. elegans* embryo, distinct by their residence time (Figure 1C).

To faithfully distinguish the number of microtubule-contact populations present at the cortex of the *C. elegans* embryo and to finely characterise them, we implemented an advanced statistical analysis of the contact duration distribution (Figure 1D). This offers

improvements with respect to published approaches on four aspects. (a) When fitting data points, whose standard errors are Gaussian-distributed, maximising the model likelihood often corresponds to least-square fitting. However, we fitted a histogram with few counts in some bins. Thus, the error distribution followed a Poisson law. Therefore, we designed the corresponding objective function (Figure 1D, grey) (Supp. Text §1.2.2) (Laurence and Chromy, 2010). (b) To distinguish between multiple microtubule-population dynamics within each embryo, and embryos with single dynamics but different from each other, we avoided averaging the data from multiple embryos but instead fitted the same model on each embryo by global fitting, i.e. maximizing the global likelihood being the product of the embryo-wise likelihoods (Figure 1D, orange) (Supp. Text §1.2.3). (c) We performed an objective selection of the best mixture-of-exponential model using the Bayesian Inference Criterion (*BIC*) (Schwarz, 1978). The number of exponentials in the best model suggests, without any hypothesis, the number of microtubule dynamical behaviours within an embryo (Figures 1D, blue) (Supp. Text §1.2.4). (d) To ensure proper comparison of the results between conditions, we computed the confidence intervals on the fitted parameters using two different approaches, bootstrapping and likelihood ratio (Bolker, 2008; Agresti, 2013) (Figures 1D, purple) (Supp. Text §1.2.5). Applying this approach to untreated embryos of *C. elegans*, we found two dynamical behaviours for the microtubule contacts at the cortex (Figure 1EF).

We reasoned that supporting models featuring more parameters needs more data points to be selected by methods like the Bayesian Inference Criterion. We thus set to explore whether a third population with a very-short or very-long lifetime might exist. A very-short-lived population may correspond to astral microtubules growing, touching and immediately leaving because they are neither captured by a motor (dynein) nor stabilised by a MAP (Janson *et al.*, 2003). However, the triple-exponential model fitting rather suggests a longer lifetime for the third population (Table S2). Furthermore, microtubules performing touch-and-go at the cortex are not likely to contribute to cortical force generation there. The triple-exponential model suggested the possible presence of a 4 s lifetime third population, however with a proportion below 4%. Biologically, some microtubules could be stabilised at the cortex (Sugioka *et al.*, 2018) or stalled there (Hendricks *et al.*, 2012; Laan *et al.*, 2012a; Laan *et al.*, 2012b). We asked whether the ~20 000 microtubule contacts per embryo in the experimental data are sufficient to support the detection of a putative third population and addressed this question *in silico* (Supp. Text §2.2.2). We fabricated embryo data simulating contacts, referred as "*fabricated embryos*", with three dynamical behaviours of lifetimes 0.4 s, 1.5 s and 4 s, and population proportions set to 55%, 40% and 5%, respectively. To mimic the experimental investigations of a given condition, here untreated embryos, we generated 10 "*simulated samples*", composed of 25 fabricated embryos, which we analysed using the DiLiPop statistical assay. A sample size of 20 000 tracks or more per embryo was necessary for the triple-exponential model to be selected as the best one in most of the fabricated samples (Supplemental Figure S1D). Larger sample sizes enabled more accurate model-parameter estimates. Our experimental data thus contained enough tracks to allow identifying a putative third population. We reckoned that another limitation precluding the detection

of a third population could be its small proportion and set to determine *in silico* the minimum requirement. We fabricated embryos with 20 000 tracks for each and three populations of lifetimes 0.4 s, 1.5 s and 4 s, the proportion of the short-lived population was kept to 55% and the third population one ranged from 2.5% to 10%. We found that third-population proportions at least equal to 5% were necessary to support the triple-exponential model as preferred one (Supplemental Figure S1E). We concluded that in untreated embryos, there is few (less than 5%) or no very-long-lived population of astral microtubules, contributing little or no to cortical force generation. Finally, we asked whether the dual-exponential dynamics of the microtubule contacts correspond to two well-defined astral microtubule populations or may reflect a broad variety of dynamical behaviours. This latter case corresponded to the stretched-exponential model and was excluded by the model selection criterion (Table S2) (Lee *et al.*, 2001; Siegel *et al.*, 2001), but we asked once again whether the amount of experimental data may have allowed identifying such a case. By *in silico* investigation, using fabricated embryos with contacts displaying a stretched exponential behaviour of lifetime 0.1 s and power 2.2, we found that 500 tracks were sufficient (Supp. Text §2.2.1), although a larger number increased the accuracy of recovered parameters (Supplemental Figure S1E). Because we had much more tracks in experimental data, we concluded that the two dynamical behaviours measured *in vivo* really corresponded to two populations of microtubule-contact tracks.

We next asked whether the dynamical behaviours of the tracks reflect the presence of two populations of microtubules and investigated possible artefacts caused firstly by the microtubule labelling. Indeed, it was recently proposed that tubulin paralogs composition of the microtubules impacted their dynamics (Honda *et al.*, 2017) or the spindle positioning (Wright and Hunter, 2003) in the *C. elegans* one-cell embryo. Thus, we asked whether YFP::α-tubulin fluorescent labelling could create two populations. We performed a similar DiLiPop analysis in GFP::β-tubulin-labelled embryos and measured two dynamical behaviours again at the cortex, with characteristic lifetimes very similar to the ones obtained with α-tubulin labelling (Figure 2A). We concluded that the two dynamically-distinct microtubule populations do not depend on a specific entire-microtubule labelling.

To complete artefact exclusion, we challenged the image-processing pipeline in two ways. Firstly, and in contrast with simulations of tracks durations above, we fabricated images containing particles with a single dynamical behaviour (Figure 2E, 2F black, Table S3). By DiLiPop analysis of *in silico* images, we recovered the mono-exponential as the best model, with the correct parameters (Figure 2F, red). In contrast, when we performed a similar simulation with two dynamical behaviours, we recovered double-exponential as best model and accurate parameters (Figure 2G, blue). Overall, this suggests that the KUT image-processing pipeline used here performed without causing artefacts. Secondly, and to gain certainty, we repeated the analysis on *in vivo* data using a different image-processing pipeline composed of algorithms based on different hypotheses. This pipeline, named NAM, encompasses the ND-SAFIR denoising (Boulanger *et al.*, 2010) (Figure 2D2), the ATLAS spot-detecting (Basset *et al.*, 2015), and the MHT linking

(Multiple Hypothesis Tracker) (Reid, 1979) (Figure 2D3). Corresponding settings are listed in Table S4 (Supp. Text §2.1.1). Applied to untreated *C. elegans* embryos, the NAM pipeline combined to DiLiPop statistical analysis produced results similar to the KUT pipeline (Figure 2C). Therefore, the two dynamical behaviours suggested by the analysis are not artefactual.

Finally, to test whether this double dynamical behaviour of microtubule cortical contacts is specific to C. *elegans*, we investigated the microtubule dynamics at the cortex in *Caenorhabditis briggsae* β-tubulin-labelled embryos, a nematode cousin of *C. elegans*, and we also observed two populations distinguished by their different dynamical behaviours (Figure 2B). We concluded that these two populations are not a peculiarity of *C. elegans* embryo. They may instead originate from conserved cortical force generation mechanisms between these two species, which share already spindle positioning systems (Riche *et al.*, 2013; Bouvrais *et al.*, 2018).

Overall, by viewing entirely-labelled microtubules, we measured two populations of astral microtubules at the cortex. There, they can generate pulling and pushing forces and in particular, pushing microtubules, in growing state, are likely to reside longer, while pulling ones coordinate dynein action, lasting about 0.5 s, with depolymerisation (Rodriguez-Garcia *et al.*, 2018). Therefore, we formulated our *two-population hypothesis,* stating that long-lived microtubules could be the pushing ones and those short-lived the pulling ones (Figure 3E).

The short- and long-lived microtubules contribute to pulling from and pushing against the cortex.

We set to test whether the short-lived population reflected the pulling-force-generating events. If so, its cortical density is expected to be polarised, especially during anaphase, to cause the spindle posterior-displacement. We refined the DiLiPop assay to measure the evolution of both microtubule populations along the mitosis and to map them in the embryo. The region and period used to perform such a block-analysis were selected to preserve sample size large enough to guarantee proper detection of the two populations (Supp. Text §1.3, Supplemental Figure S2), while the procedure to represent each population in *DiLiPop-maps* was similar to our previous one used to map all microtubules without dynamic classification (Bouvrais *et al.*, 2018). Applied to untreated *C. elegans* embryos (N = 25), this analysis recovered the high-density ridgelines of microtubule-contacts for both populations (Figure 3A), which corresponded to the centrosomal positions (Bouvrais *et al.*, 2018). Importantly, from 100 s before anaphase on, the short-lived contact-density was larger in the 70-100% region (classically measured along the anteroposterior (AP) axis) than in the anterior cortex (Figure 3A1), while the long-lived population was only slightly polarized at late anaphase, as expected because of the posterior displacement of the spindle (Figure 3A2) (Bouvrais *et al.*, 2018). The polarisation of the short-lived but almost not the long-lived population suggests that the former reflects pulling-force events.

To strengthen our two-population hypothesis, we genetically decreased or increased cortical pulling forces and observed how the spatial distribution of the short-lived-microtubule density is affected (Rodriguez-Garcia *et al.*, 2018). To do so, we respectively depleted GPR-1/2^{LGN}, the well-established force generator regulator (Colombo *et al.*, 2003; Grill *et al.*, 2003; Pecreaux *et al.*, 2006a), and CNSK-1 involved in repressing anterior forces (Panbianco *et al.*, 2008). Firstly, we treated *gpr-2(ok1179)* mutant embryos by *gpr-1/2(RNAi)* to ensure a more pronounced depletion and computed the DiLiPop-map. We observed a strong reduction in the short-lived-microtubule density in the posterior region in comparison with the control (Figure 3B1-2, Supplemental Figure S4B1) leading to an almost symmetric anteroposterior distribution, while the anterior region was mostly not affected. The slight asymmetry of the long-lived-microtubule density in late anaphase also tended to vanish (Supplemental Figure S4A2,B2), as expected since the spindle position was more centred (Supplemental Figure S5C1-2). To check on the penetrance of the GPR-1/2 depletion, we monitored the cortical pulling forces, using spindle pole oscillations and displacements, in $N = 8$ embryos treated in the same way and imaged at the spindle plane. We observed no oscillation and a strong reduction of the posterior centrosome displacement as reported previously (Supplemental Figure S5C1-2) (Colombo *et al.*, 2003; Pecreaux *et al.*, 2006a). Similarly to the above analysis, we tested *in silico* whether the number of microtubule-contacts in each region and period was sufficient to permit detecting two populations (Supplemental Text §2.2.3) and found that with $Ne = 8$ fabricated embryos and sample size of 3000 tracks, mimicking the experiments with protein depletion, lifetime difference T_2-T_1>0.4 s is sufficient if the proportion P_1 is between 30% and 70%, else T_2-T_1>1 s is required (Supplemental Figure S3B-G). We concluded that the short-lived-population distribution strongly depends on GPR-1/2 supporting that these microtubules contribute to pulling force generating.

Secondly, we performed the converse experiment, enriching the force generators anteriorly through a *cnsk-1(RNAi)* treatment (Panbianco *et al.*, 2008). Computing the DiLiPop map, we observed an increase in the short-lived microtubule-contact densities anteriorly, compared to controls (Figure 3B3, Supplemental Figure S4B1), as expected. We also observed a slight decrease in the short-lived microtubule-contact densities at the posterior crescent attributed to the anterior displacement of the spindle (Supplemental Figure S4B1, S5C1,3) (Bouvrais *et al.*, 2018; Rodriguez-Garcia *et al.*, 2018). The long-lived microtubule density overall increased possibly because an altered actin-myosin network is indirectly affecting microtubule dynamics (Severson and Bowerman, 2003; Redemann *et al.*, 2010) or because of a more direct CSNK-1 dependent change in microtubule dynamics (Fievet *et al.*, 2013) (see also micrographs in (Panbianco *et al.*, 2008)) (Supplemental Figure S4A3,B2). To check on the penetrance of our treatment, we imaged $N = 9$ similarly *cnsk-1(RNAi)*-treated embryos at the spindle plane and observed mildly increased oscillations at the posterior pole, with a peak-to-peak amplitude of 8.10 ± 1.99 µm compared to 6.43 ± 1.89 µm ($p = 0.079$), and more substantially increased ones anteriorly, 6.64 ± 0.76 µm compared to 2.66 ± 0.84 µm in control embryos ($p = 7.5\times10^{-9}$), confirming the significant increase in pulling forces mostly at anterior (Panbianco *et al.*, 2008). Overall, the short-lived-microtubule density correlates with the

cortical force intensity and the number of force generators (Grill *et al.*, 2003; Panbianco *et al.*, 2008; Rodriguez-Garcia *et al.*, 2018), supporting our two-population hypothesis.

Our hypothesis also suggests that the long-lived microtubules correspond to cortical-pushing events. To support this view, we investigated the two cortical-contact populations upon genetically altering the dynamics of the microtubules and then studied microtubule dynamics using an EB-labelling.

Firstly, we impaired microtubules growing by depleting the microtubule polymerase ZYG-9$^{XMAP-215}$ by RNAi (Figure 3C1) and performed a DiLiPop analysis during metaphase considering all regions. We found two populations but interestingly, only the long-lived microtubules had their lifetime reduced while the short-lived one was unaltered (Figure 3C2-3, green). This was consistent with the microtubule polymerase activity of ZYG-9 (Brouhard *et al.*, 2008) and supported our hypothesis that the long-lived population accounts for growing microtubules. We checked on the penetrance by repeating the experiment and imaging at the spindle plane. We observed, during the centring establishment, an incomplete anterior displacement of the spindle, which reached 0.63 ± 0.85 µm upon *zyg-9(RNAi)* (N = 10) compared to – 0.7 ± 0.5 µm in control embryos (N = 13, $p = 6.5\text{x}10^{-4}$). This phenotype was expected and confirmed the ZYG-9 penetrance (Grill *et al.*, 2001). To confirm that the observed alteration of the long-lived microtubule dynamics corresponds specifically to a perturbation of the growth rate and not to generic altered dynamics, we depleted the microtubule depolymerase KLP-7^{MCAK} by RNAi (Figure 3C1). The DiLiPop analysis revealed no significant change in the lifetime of the long-lived population (Figure 3A2, blue). We also found that the short-lived population displayed a slightly increased residence time (Figure 3A3, blue) consistent with the increased pulling forces previously reported (Gigant *et al.*, 2017). To check on the penetrance, we repeated the experiment imaging at the spindle plane and observed, during anaphase, a faster elongation of the spindle (0.166 ± 0.056 µm/s (N = 12) compared to 0.116 ± 0.025 µm/s for the control embryos, p = 0.012) in agreement with (Bellanger *et al.*, 2007; Maton *et al.*, 2015), which confirmed KLP-7 penetrance. Both KLP-7 and ZYG-9 depletions suggest that the short-lived population may reveal the microtubules in a shrinking state while the long-lived population contains growing microtubules.

Secondly, and to strengthen the link between long-lived population and growing state, we analysed, with the DiLiPop assay, microtubules specifically in growing state, using an EBP-2::GFP strain. We found a single microtubule-contact population with an intermediate lifetime compared to the two population lifetimes found when labelling all microtubules using YFP::α-tubulin (Figure 3D1). Finding a single population is consistent with our hypothesis that the two dynamical behaviours of the microtubule-contacts correspond to distinct states. The intermediate lifetime could be attributed either to a direct effect of EB protein over-expression, increasing microtubule dynamics in other organisms (Duellberg *et al.*, 2016), or to a reduction/disappearance of the GTP cap, which concentrates EB proteins (Bieling *et al.*, 2007; Zanic *et al.*, 2009), earlier than the switch to catastrophe, making the contact disappears prematurely (Figure 3D2) (Kozlowski *et al.*, 2007). Indeed, some proteins like CLASP can stabilise the microtubule

(Espiritu *et al.*, 2012), while dynein can even clamp the microtubule ends preventing depolymerisation (Laan *et al.*, 2012a). Overall, these observations suggest that the long-lived microtubules reflect microtubules growing against the cortex, which would generate a pushing force.

Altogether, these experiments focusing mostly on the spatial distribution of the microtubules support the two-population hypothesis. On the one hand, the short-lived microtubules are likely involved in pulling-force generating and their lifetime is consistent both with dynein residence time at the cortex (Rodriguez-Garcia *et al.*, 2018) and estimates of force-generator runtimes obtained by spindle-pole oscillation modelling (Pecreaux *et al.*, 2006a). On the other hand, the long-lived microtubules include those growing against the cortex, thought to generate the pushing forces maintaining the spindle in cell-centre during metaphase. Indeed, their residence time agrees with the estimation coming from centring stability measurements (Pécréaux *et al.*, 2016) (Figure 3E).

The polarised short-lived-population density, reflecting dynein on-rate, accounts for the pulling force imbalance and the final spindle position.

Our recent study of dynein dynamics at the embryo cortex suggested that force imbalance is caused by a higher dynein-binding rate of the cortical force generators at the posterior cortex compared to anterior one (Rodriguez-Garcia *et al.*, 2018). Equipped with the DiLiPop assay, we aimed to go beyond and investigate how the pulling forces are regulated along time since the short-lived microtubules reveal them. We performed the analysis using 60 s time-windows and found a higher density of short-lived posteriorly from the beginning of our recording corresponding to prometaphase (Figure 4A), while the lifetime remained symmetric during metaphase and mostly during anaphase (Figure 4B). These results support that polarity is reflected by a force generator on-rate imbalance (Rodriguez-Garcia *et al.*, 2018). Furthermore, this density ratio got more significantly pronounced during anaphase, when most of the posterior displacement of the spindle intervenes, consistent with the increase in the cortical pulling imbalance along metaphase and anaphase previously proposed at the cellular level in (Labbé *et al.*, 2004). Interestingly, the long-lived population, despite it is not involved in pulling, became also posteriorly enriched, but only at late anaphase (Figure 4C), while its lifetime stayed close to the symmetry all the time (Figure 4D). We attributed this to the posterior displacement of the spindle (Bouvrais *et al.*, 2018). Such a "geometrical" effect, reported to reinforce the posterior force generator engagement upon displacement of the centrosome (Bouvrais *et al.*, 2018), would account at least for a part of the density increase in the short-lived population with mitotic progression.

We wondered to which extent it causes the asymmetric short-lived microtubule density. To address this question, we performed a time-resolved DiLiPop analysis of CSNK-1 depleted embryos. This protein acts upstream polarity mechanism mostly limiting the pulling forces generated anteriorly (Panbianco *et al.*, 2008). We found that the long-lived population became asymmetrically distributed during late anaphase (Supplemental Figure

S5B1,3), consistent with the almost normal posterior displacement of the posterior centrosome (Supplemental Figure S5C1,3), but the distribution of the short-lived population was symmetric (Supplemental Figure S5A1,3). This excludes that the asymmetrical short-lived-microtubule density could be caused only by a geometrical effect.

We set to go beyond our previous study relating the rate of dynein microtubule-binding/engaging in pulling and the force imbalance (Rodriguez-Garcia *et al.*, 2018), and asked whether some additional mechanism could contribute to reflect polarity into force imbalance. In particular, it was proposed that microtubule dynamics to the force imbalance and the posterior displacement of the spindle (Kozlowski *et al.*, 2007). Interestingly, EFA-6 negatively regulates the force generator, dynein, and microtubule dynamics (O'Rourke *et al.*, 2007; O'Rourke *et al.*, 2010). DiLiPop analysis of *efa-6(RNAi)* showed a modest increase in the short-lived-microtubule density leading to a delay in the appearance of an anteroposterior asymmetry and a strong increase in the long-lived-population density (Supplemental Figure S5A1,4;B1,4). Repeating the experiment in the same conditions at the spindle plane, we observed as expected a reduction in anaphase oscillations, the peak-to-peak oscillation of the posterior centrosome being equal to 2.58 ± 2.71 μm (N = 12) compared to 6.43 ± 1.89 μm for control embryos (N = 9, p = 0.001) but an exaggerated posterior displacement (Supplemental Figure S5C1,4) (O'Rourke *et al.*, 2010). This is consistent with an increase in centring forces that also dampen the oscillations, especially on the transverse axis because the embryo oblong shape decreases these forces along the anteroposterior axis (Howard, 2006; Pecreaux *et al.*, 2006a; Garzon-Coral *et al.*, 2016; Pécréaux *et al.*, 2016). In contrast, the pulling forces only mildly increase on the posterior during anaphase. This, in addition to the long-lived population being symmetric, suggests that the long-lived population opposed to the cortical pulling forces, supporting the hypothesis that only the short-lived population reflects the polarity.

To gain certainty, we analysed, through the DiLiPop assay, the two-population phenotype after depleting proteins controlling the density of the pulling force generators, as reflected by short-lived population, and upstream polarity proteins. Firstly, we depleted GPR-1/2^{LGN}, LIN-5^{NuMA} and Gα proteins, which are components of the trimeric force generator and its cortical anchorage module. We found that the density imbalance was abolished until mid-anaphase, and was strongly reduced thereafter upon *gpr-2(ok1179);gpr-1/2(RNAi), lin-5(RNAi)* and *goa-1;gpa-16(RNAi)* (Supplemental Figure S5A1-2, Supplemental Figure S6A,). As expected, the long-lived population showed no asymmetry under these treatments (Supplemental Figure S5B1-2, Supplemental Figure S6B), because the spindle posterior-displacement was reduced (Supplemental Figure S5C1-2, Supplemental Figure S6C). To confirm the efficiencies of these depletions, we imaged embryos in the same conditions at the spindle plane and noticed no spindle pole oscillation and a reduced spindle posterior-displacement and elongation (Supplemental Figure S5C1-2, Supplemental Figure S6C). Importantly, *par-3(RNAi)* and even more strongly *par-2(RNAi)* resulted in a reduction in the density imbalance of the short-lived-

population (Supplemental Figure S7A). We confirmed the PAR-protein depletion efficiencies by imaging similarly treated embryos at the spindle plane and observed divisions closed to the symmetry for both depletions, with an increased anterior displacement after depleting PAR-3 and a reduced posterior displacement after depleting PAR-2 (Supplemental Figure S7B), as expected (Grill *et al.*, 2001). We concluded that the PAR proteins related polarity is likely and only reflected by the short-lived-population density, necessary and sufficient to translate polarity into force imbalance.

To strengthen this hypothesis, we asked whether the final position of the spindle, measured by imaging at the spindle plane and tracking the centrosomes, correlated with the asymmetric density of the short-lived population, obtained from DiLiPop analysis after imaging at the cortex plane, in control and genetically perturbed embryos. We plotted the final spindle position along the AP axis (*Sx* (Pécréaux *et al.*, 2016)) versus the anterior (0-45% of AP axis) to posterior (70-100% of AP axis) density ratio of the two populations during anaphase. We obtained a more pronounced correlation using the short-lived-microtubule density-ratio compared to the long-lived-population one (Figure 4EF). Interestingly, the spindle centred position, $Sx = 50\%$, corresponded – through a linear fit estimate of density ratio – to a ratio equal to 1.035 for the short-lived population (Figure 4E, dotted line), suggesting quasi-equal pulling from anterior and posterior cortices. We concluded that the pulling force imbalance is recapitulated by the asymmetric density ratio of the short-lived population. In turn, this density corresponds to the binding rate of force generator dynein to the microtubule or to the initiation of a molecular motor run to exert a pulling force (globally termed on-rate (Rodriguez-Garcia *et al.*, 2018)). By combining cell-scale and single-component measurements, we can overall conclude that polarity is translated into a force imbalance solely by this asymmetric on-rate.

The short-lived-microtubule lifetime reflects the mitotic progression control through the force generator processivity.

A temporal control of the cortical pulling forces was previously reported (McCarthy Campbell *et al.*, 2009) and, based on cell-scale measurements during anaphase, we suggested that it acted through the force generator processivity, reflected into the short-lived-microtubule lifetime (Pecreaux *et al.*, 2006a; Bouvrais *et al.*, 2018). We sought a direct proof of such a regulation and studied the temporal evolution of the two-population residence times using a time resolution window of 30 s, which still ensured accurate estimates. We found a steep increase in the short-lived-microtubule lifetime during the early anaphase, continued by a shallower one in late anaphase, in contrast to a constant lifetime during metaphase (Figure 5A). This observation, consistent with an increase in force generator processivity during anaphase, brings for the first time a direct observation of this at the single-microtubule scale. Furthermore, it raised the question of whether this corresponds to a force control mean or to a bare consequence of some other process. Interestingly, we observed that the long-lived-microtubule lifetime undergoes the same time evolution but with a reduced amplitude variation, (Figure 5B). This suggests that some distinct processes might regulate each microtubule population.

The short-lived-population lifetime would increase beyond the consequence of the bare increased microtubule-nucleation rate (Srayko *et al.*, 2005) or of the posterior displacement, which makes more microtubules available at the cortex (Bouvrais *et al.*, 2018).

The polymerising microtubules, viewed in the long-lived population, contribute to maintaining the spindle in the cell-centre.

We recently proposed that microtubule pushing against the cortex contributes to maintaining the spindle in the cell centre during metaphase (Garzon-Coral *et al.*, 2016; Pécréaux *et al.*, 2016). However, other mechanisms were proposed, involving pulling from either the cortex or the cytoplasm (Grill and Hyman, 2005; Kimura and Kimura, 2011a; Kimura and Kimura, 2011b; Shinar *et al.*, 2011; McNally, 2013; Barbosa *et al.*, 2017). We set to investigate how the long-lived population of microtubules varied upon various genetic perturbations of microtubule dynamics, to discriminate between those hypotheses. We used the stability of the metaphasic spindle in the cell centre as a readout of the centring (Pécréaux *et al.*, 2016): this is recapitulated into the diffusion coefficient D_{Sy} of the spindle along the transverse axis. The larger this value, the poorer the stability. This value was computed from imaging at the spindle plane. We found a strong anti-correlation between the diffusion coefficient and the density of long-lived microtubules (Figure 6A) but not with the short-lived-population density (Supplemental Figure S8A). These observations suggest that microtubule pushing rather than pulling contributes to maintaining the spindle in the cell centre. Furthermore, because the microtubule density at the cortex impacted the centring, these results are not consistent with the cytoplasmic pulling hypothesis. We also found an anti-correlation between the centring stability and the long-lived-population lifetime (Figure 6B) as expected, since longer pushing improves the centring (Howard, 2006; Pécréaux *et al.*, 2016). Interestingly, the short-lived-microtubule lifetime anti-correlated also with the centring stability (Supplemental Figure S8B), in contrast to the density, consistent with the stochastic attachment and detachment of the cortical pulling force generators creating noise that perturbs the centring: higher dynamics of force generators leading to poorer stability (Pécréaux *et al.*, 2016). Through direct observation of pushing force events, we conclude that the spindle is likely maintained at cell centre during metaphase by microtubule pushing against the cortex, while the pulling events add some biological noise.

DISCUSSION

Through an advanced and careful analysis of microtubule-contact dynamics at the cortex of *C. elegans* embryos, based on high frame-rate imaging, we could for the first time resolve two microtubule populations, distinct by their residence time. Measured as 0.4 s and 1.8 s, these lifetimes are rather short with respect to previously published values, which range between 1 s and 15 s (Labbé *et al.*, 2003; Kozlowski *et al.*, 2007; Gerhold *et al.*, 2018; Sugioka and Bowerman, 2018). These differences could be attributed to different microtubule labellings, growing microtubule plus-end or whole microtubule,

mitotic phase considered, or various sample-mounting techniques. Noticeably, approaches with higher frame rate, consistent with microtubule growth and shrink rates, provide smaller residence times, close to the values found here. Furthermore, and key to DiLiPop out-performing existing methods, the imaging and tracking ensure the capture of a much larger number of microtubule contacts, ensuring strong representative statistics. Finally, the DiLiPop advanced and tailor-made statistical analysis enables to disentangle mixed dynamics in a set of microtubule-contact durations.

Towards a multi-scale approach by combining the DiLiPop assay with cell-scale investigations.

One decisive trait of our approach is the combining of measurements at cell scale and single-microtubule scale (microscopic). In particular, it enables us to understand the spatial and temporal regulation of the cortical pulling forces as well as support our hypothesis of spindle maintenance in the cell centre by microtubule pushing. Firstly, and because short- and long-lived microtubules reflect pulling and pushing force generating events, respectively, our assay enables for the first time to delineate the concomitant time and space evolution of these forces at the microscopic level, paving the way to understand how it accounts for the complex choreography of the mitotic spindle. In particular, we confirmed that the asymmetry in pulling forces – visible here through the density of the short-lived population – was encoded as an imbalance in dynein binding rate rather than in dynein detachment rate, as proposed in (Rodriguez-Garcia *et al.*, 2018). Secondly, and superseding our study focusing on dynein, we suggest that no other mechanism downstream of polarity proteins PAR-2/-3 and CSNK-1 contributes significantly to the pulling force imbalance. The time evolution of the short-lived-microtubule densities suggests that their asymmetric distribution, thus the force imbalance, is present from early prometaphase, as previously inferred from cell-scale measurements (Labbé *et al.*, 2004). Thirdly, the pulling force amplitude – related to the force-generator persistence pulling (processivity) based on modelling cell-scale centrosome kinematics (Pecreaux *et al.*, 2006a) – viewed here through the cortical residence time of the short-lived microtubule, stays in contrast at constant value until anaphase onset, when it starts increasing with time, while the spindle migrates posteriorly and elongates due to the cortical pulling forces. Fourthly, observing that the spindle stability in the cell-centre during metaphase correlates with the density of pushing microtubules at the cortex, reflected by the long-lived population, we suggest that these pushing microtubules contribute to the centring-maintenance mechanism.

The short-lived population might not account for only pulling events.

Measuring the displacement of centrosome fragments after laser disintegration suggests that twice more force generators are active at the posterior cortex (Grill *et al.*, 2003) while the anterior-to-posterior density-ratio of the short-lived microtubules is above 0.5. It suggests that some of these short-lived contacts might represent microtubules not involved in pulling events. Interestingly, analysing the dynein dynamics at the cortex led

to a similar ratio (Rodriguez-Garcia *et al.*, 2018). It could correspond to stalled microtubule-ends/dyneins. Indeed, *in vitro* and *in vivo* studies showed that anchored dynein could serve as microtubule plus-end tether (Dujardin and Vallee, 2002; Hendricks *et al.*, 2012; Laan *et al.*, 2012b; Perlson *et al.*, 2013; Yogev *et al.*, 2017). Consistently, the number of short-lived microtubules contacting the cortex is a bit large compared to the expected values of 10-100 per cortex half (Grill *et al.*, 2003; Redemann *et al.*, 2010). Indeed, we measured, during late anaphase, about 40 short-lived microtubules contacting the visible cortex each second, extrapolating to about 120 per half cortex. A fraction of these could be stalled dynein tethering the microtubule ends. This can be the signature of a mechanism regulating dynein run initiation from a state where it captures the microtubule (Laan *et al.*, 2012a; Jha *et al.*, 2017).

Microtubules pushing against the cortex likely perform the centring maintenance.

The spindle was proposed to be maintained in the cell centre by three families of mechanisms: pushing forces generated by microtubule growth against the cortex, similarly to what was found in yeast e.g.; the pulling on astral microtubules from the cortex, carefully regulated in space; and forces generated within the cytoplasm by force generators attached on small organelles (Reinsch and Gonczy, 1998; Grill and Hyman, 2005; Kimura and Onami, 2005; Wühr *et al.*, 2009; Zhu *et al.*, 2010; Kimura and Kimura, 2011b; Kimura and Kimura, 2011a; Shinar *et al.*, 2011; Laan *et al.*, 2012a; McNally, 2013; Garzon-Coral *et al.*, 2016; Pécréaux *et al.*, 2016; Barbosa *et al.*, 2017; Wu *et al.*, 2017). Because the dynamics of microtubules at the cortex correlate with the centring stability, our finding is poorly consistent with cytoplasmic pulling. Furthermore, during metaphase, the density of long-lived – but not the short-lived – microtubules anti-correlates with the centring stability, consistently with centring by pushing. Interestingly, the short-lived-population density was low during that period, indicating that it likely does not contribute to centring. As previously suggested, pulling forces revealed by short-lived population contribute to de-centring and are down regulated during metaphase to let the spindle maintain in cell centre (Dogterom *et al.*, 2005; Grill and Hyman, 2005; Zhu *et al.*, 2010; Pécréaux *et al.*, 2016). Noticeably, we found no polarisation of the long-lived population, beyond the density imbalance due to the spindle displacement in late anaphase. Out of the scope of this work, our multi-scale approach could also be used to decipher centring establishment prior to mitosis (Ahringer, 2003) and the orientation of the pronuclei-centrosome complex (PCC), for which the mechanisms are still debated (Tsou *et al.*, 2003b; Labbé *et al.*, 2004; Kimura and Onami, 2005, 2007; Park and Rose, 2008; Gusnowski and Srayko, 2011; Kimura and Kimura, 2011a; Kimura and Kimura, 2011b; Barbosa *et al.*, 2017).

The short-lived-microtubule density reflects positional regulation while its lifetime the mitotic progression.

We recently proposed that the cortical pulling forces are regulated both by the position of the centrosome, which in turn controls the amount of microtubules that can be captured by the cortical force generators on the one hand, and on the other hand, by the processivity of the force generators increasing along time (Pecreaux *et al.*, 2006a; Bouvrais *et al.*, 2018). Our assay here offers the unique opportunity to observe separately these two, as the former controls the density of pulling microtubules and the later their lifetime. Indeed, the time evolutions of the density of short-lived and long-lived microtubules are quite alike and thus suggest a global control by the position. The cell cycle control of the number of nucleated microtubules, known to increase at anaphase (Srayko *et al.*, 2005), will further reinforce this density increase at that moment. Noticeably, we found both long-lived and short-lived microtubules at the cortex along the whole mitosis, including when the short-lived ones are limiting the number of engaged force generators since force-generator to microtubule attachment corresponds to a pseudo-chemical reaction as modelled in (Bouvrais *et al.*, 2018). This is because the force generators or their anchor sites are in limited number and thus sparse at the cortex (Grill *et al.*, 2003; Grill *et al.*, 2005; Redemann *et al.*, 2010; Rodriguez-Garcia *et al.*, 2018). Consequently, not all microtubules can find a force generator to pull on (Bouvrais *et al.*, 2018). In contrast, the lifetime evolutions along metaphase and anaphase are different for short- and long-lived microtubules, suggesting that a specific mechanism regulates the short-lived-microtubule lifetime as previously suggested based on modelling at cell scale (Pecreaux *et al.*, 2006a; Bouvrais *et al.*, 2018).

In contrast to previous studies measuring the resulting forces on the centrosome along time (Grill *et al.*, 2003; Labbé *et al.*, 2004), the DiLiPop enables to separate the contributions of pulling and pushing over time, in a physiological context. While time evolutions of the densities of the both populations, reflecting both forces, are similar excluding a different mechanism of regulation, the short-lived-microtubule lifetime undergoes a more pronounced increase in anaphase compared to long-lived one. It suggests that this controls the transition between metaphase – with dominant pushing forces maintaining the spindle in the cell centre – and anaphase when pulling dominates to displace the spindle posteriorly. While the pulling increases at the latter stage, the pushing, thus the centring remains mostly constant or even slightly increases. In contrast, the pulling force plateau (constant residence time) during metaphase ensures the slow posterior displacement but lets the centring forces dominate (Ahringer, 2003; Garzon-Coral *et al.*, 2016; Pécréaux *et al.*, 2016). This regulation through intensifying the pulling/displacement forces contrasts with recent finding in sea urchin zygote where a reduction of the centring forces accounts for the decentration after the maintenance in cell-centre (Sallé *et al.*, 2018).

Which molecular mechanisms could regulate these forces?

Three forces and regulations are involved in controlling the spindle positioning: a spatial asymmetry of cortical pulling, reflecting polarity; a time increase of the same, corresponding to mitotic progression; and a constant centring. Firstly, the limited

amount of force generator regulators, GPR-1/2, or anchor sites e.g. G α proteins GOA-1/GPA-16, more abundant on the posterior side, is the most likely to account for the asymmetric density (Grill *et al.*, 2003; Pecreaux *et al.*, 2006a; Wu and Rose, 2007; Park and Rose, 2008; Riche *et al.*, 2013; Rodriguez-Garcia *et al.*, 2018). Restricting the pulling force-generators to a posterior-most crescent through LET-99 reinforces this asymmetry, and consistently we found a density of short-lived microtubules in the 45-70% similar to the anterior side (Figure 4A) (Krueger *et al.*, 2010; Bouvrais *et al.*, 2018). Recently, the APR-1/APC complex was suggested to decrease the cortical forces anteriorly (Sugioka *et al.*, 2018). Since we do not see an increase in growing microtubules anteriorly, the balance between stalled (for a short while) and shrinking microtubules, all reflected by the short-lived population, could be different between anterior and posterior, with a larger proportion of stalled microtubules anteriorly. Finally, the denser actin-myosin cortex at the anterior cortex could play a similar regulatory role (Goulding *et al.*, 2007; Colin *et al.*, 2018). Secondly, the pulling forces are regulated along the mitosis as discussed above. The first and obvious possible player is dynactin, known to be essential to cortical pulling forces and able to make dynein more processive (Skop, 1998; Gonczy *et al.*, 1999; King and Schroer, 2000; Rodriguez-Garcia *et al.*, 2018). Beyond, some other players were involved in other systems *in vitro* or *in vivo*, for example: the end-binding (EB) proteins putatively involved in initiating dynein pulling once a microtubule is captured (Jha *et al.*, 2017), and whose homolog EBP-2 contributes, although modestly, to cortical forces (Rodriguez-Garcia *et al.*, 2018); LIS-1 essential for spindle positioning in nematode and reported to be also implicated in dynein regulation beyond its classic inhibitory role (Cockell *et al.*, 2004; Baumbach *et al.*, 2017; DeSantis *et al.*, 2017); BICD-1^{BICD2} involved in nuclear migration in nematode hypodermis (Fridolfsson *et al.*, 2010) but no strong early embryonic phenotype was reported, despite indication of its role in other organisms (Swan *et al.*, 1999; Splinter *et al.*, 2012; Jha *et al.*, 2017; Urnavicius *et al.*, 2018). Thirdly and finally, efficient pushing by microtubules against the cortex requires some microtubule-associated proteins to prevent the switch to catastrophe (Janson *et al.*, 2003). Viewing of microtubule buckling in nematode suggests that microtubules are able to efficient pushing (Kozlowski *et al.*, 2007) although the involved proteins are still not clearly known. One possibility is CLS-2^{CLASP} reported to affect spindle positioning (Espiritu *et al.*, 2012). Indeed, the inability to separate the measurements of pulling and pushing forces limited the ability to delineate the involved players and this work may help to work around this issue.

Beyond these findings, this work is also a rare example of combining investigations at two scales to decipher some key mechanisms regulating mitosis, especially the forces responsible for positioning the mitotic spindle (Figure 7). It offers the unparalleled ability to view the pulling and pushing force-generating events directly, through the short-lived and long-lived microtubule contacts, and to explore the regulation of these forces in time and space. We expect that this novel approach will find applications beyond that work and that the DiLiPop tool will be used in another context, in which an experimental distribution has to be fitted, for instance in photon count experiments.

MATERIALS AND METHODS

Culturing C. elegans

C. elegans nematodes were cultured as described in (Brenner, 1974), and dissected to obtain embryos. The strains were maintained at 25°C and imaged at 23°C. The strains were handled on nematode medium plates and fed with OP50 bacteria.

Strains of C. elegans and C. briggsae used

C. elegans TH65 YFP::TBA-2 (α-tubulin) strain (Srayko *et al.*, 2005) having a fluorescent labelling of the whole microtubule (MT) was used for the DiLiPop assay as well as *C. elegans* AZ-240 GFP::TBB (β-tubulin) strain (Praitis *et al.*, 2001) and *C. briggsae* ANA020 GFP::TBB (β-tubulin) strain. TH27 TBG-1::GFP (γ-tubulin) strain (Oegema *et al.*, 2001) displaying a centrosomal fluorescent labelling was the standard for the "centrosome-tracking" assay. TH66 EBP-2::GFP strain (Srayko *et al.*, 2005) that displays a labelling of microtubule plus-ends was used for comparison of its effects on microtubule dynamics. The JEP-18 *gpr-2(ok1179)* strain was used to target GPR-1/2 protein though a mutation.

Gene inactivation through protein depletion by RNAi feeding

RNA interference (RNAi) experiments were performed by feeding using the Ahringer-Source BioScience library (Kamath and Ahringer, 2003), except for GOA-1;GPA-16 depletion, whose clone was kindly given by Prof P. Gönczy. The feedings were performed at 25°C for various durations according to the experimental goals. The treatment lasted 24h for *lin-5*, *goa-1*;*gpa-16, efa-6* and *klp-7* genes. When we aimed for stronger phenotypes (e.g. symmetric divisions), we used duration of 48h (*cls-2*, *par-2*, *par-3* and *gpr-1/2*). The duration was reduced to 4h and 6-10h when targeting *zyg-9* and *cnsk-1*, respectively. The control embryos for the RNAi experiments were fed with bacteria carrying the empty plasmid L4440. We did not notice any phenotype suggesting that the meiosis was impaired during these various treatments.

Preparation of the embryos for imaging

Embryos were dissected in M9 buffer and mounted on a pad (2% w/v agarose, 0.6% w/v NaCl, 4% w/v sucrose) between a slide and a coverslip. Depending on the assay (landing or centrosome-tracking ones), embryos were observed using different microscopic setups. To confirm the absence of phototoxicity and photodamage, we checked for normal rates of subsequent divisions (D.L. Riddle, 1997; Tinevez, 2012). Fluorescent lines were imaged at 23°C.

Imaging of microtubule contacts at the cortex

We imaged *C. elegans* one-cell embryos at the cortex plane in contact with the glass slide, viewing from the nuclear envelope breakdown (NEBD) until late anaphase. We used a Leica DMi8 spinning disk microscope with Adaptive Focus Control (AFC) and a HCX Plan Apo 100x/1.4 NA oil objective. Illumination was performed using a laser with emission wavelength of 488 nm and we used GFP/FITC 4 nm band pass excitation filter

and a Quad Dichroic emission filter. To account for the fast microtubule dynamics at the cortex, images were acquired at an exposure time of 100 ms (10 Hz) using an ultra-sensitive Roper Evolve EMCCD camera that was controlled by the Combox. During the experiments, the embryos were kept at 23°C. To image embryos at the cortex, we typically moved the focus to 12 to 15 μm below the spindle plane. Images were then stored using Omero software (Li *et al.*, 2016).

Spindle pole imaging

Embryos were observed at the midplane using a Zeiss Axio Imager upright microscope modified for long-term time-lapse. First, an extra anti-heat filter was added to the mercury lamp light path. Secondly, to decrease the bleaching and obtain optimal excitation, we used an enhanced transmission 12 nm band pass excitation filter centred on 485 nm (AHF analysentechnik). We used a 100x/1.45 NA Oil plan-Apo objective. Images were acquired with an Andor iXon3 EMCCD 512x512 camera at 33 frames per second and using their Solis software. Images were then stored using Omero software (Li *et al.*, 2016).

Centrosome-tracking assay

The tracking of labelled centrosomes and analysis of trajectories were performed by a custom tracking software (Pecreaux *et al.*, 2006a) and developed using Matlab (The MathWorks). Tracking of -20°C methanol-fixed γ-tubulin labelled embryos indicated accuracy to 10 nm. Embryo orientations and centres were obtained by cross-correlation of embryo background cytoplasmic fluorescence with artificial binary images mimicking embryos, or by contour detection of the cytoplasmic membrane using background fluorescence of cytoplasmic TBG-1::GFP with the help of an active contour algorithm (Pecreaux *et al.*, 2006b). The results were averaged over all of the replicas for each condition.

Simulation of microscopy images

To validate the image processing pipeline, we fabricated fluorescence images of known dynamics, which mimic our cortical images using the algorithm developed by (Costantino *et al.*, 2005) that we adapted to our needs. In further details, we simulated stochastic trajectories of particles (Figure 2E1) that displayed a limited random motion: $x_{i,j}(t+1) = x_{i,j}(t) + \xi\,(2Dt)^{1/2}$, where $x_{i,j}(t)$ represent the coordinates in two dimensions at time t, ξ is a random number and D is the diffusion coefficient. The duration of the tracks (i.e. their length) was sampled from an exponential distribution. The intensity was set similar to experimental ones and encoded by the quantum yield parameter (Qyield). We then plotted the instantaneous positions and applied a Gaussian filter to mimic the effect of the point-spread function (PSF) in fluorescence microscopy. Then, we mimicked the background noise by adding at each pixel a sampling of a Gaussian distribution normalized to ε, with formula reading $A_{\text{noisy}} = A + \varepsilon M$ and corresponding to a SNR $\max(A)/\varepsilon$ (Figure 2E2). This simulation provided a realistic scenario to test the image-processing pipeline. Details of the parameters used for simulation can be found in Table S3.

Statistics

For classic statistical analyses (excluding model parameter comparison), averaged values of two conditions were compared using the two-tailed Student's t-test with correction for unequal variance except where otherwise stated. For the sake of simplicity, we recorded confidence levels using stars (*, $p \leq 0.01$; **, $p \leq 0.001$; ***, $p \leq 0.0001$; ****, $p \leq 0.00001$) and n.s. (non-significant, $p > 0.01$; sometimes omitted to save room). We abbreviated standard deviation by SD, standard error by s.e., and standard error of the mean by s.e.m.

Data and image processing

All data analysis was developed using Matlab (The MathWorks).

ACKNOWLEDGMENTS

The bacterial clone of GPA-16;GOA-1 was a kind gift from Prof P. Gönczy. We thank Dr. Gregoire Michaux for the feeding clone library and technical support. We also thank Drs. Anne Pacquelet, Giulia Bertolin, Xavier Pinson, Grégoire Michaux, Sébastien Huet and Marc Tramier for discussions about the project. Some strains were provided by the Caenorhabditis Genetics Center (CGC), which is funded by National Institutes of Health Office of Research Infrastructure Programs (P40 OD010440; University of Minnesota).
J.P. was supported by a Centre National de la Recherche Scientifique (CNRS) ATIP starting grant and La Ligue nationale contre le cancer. We also acknowledge Plan Cancer grant BIO2013-02, COST EU action BM1408 (GENiE) and La Ligue contre le cancer (comités d'Ille-et-Vilaine et du Maine-et-Loire). Microscopy imaging was performed at the Microscopy Rennes Imaging Center, UMS 3480 CNRS/US 18 INSERM/University of Rennes 1. Spinning disk microscope was co-funded by the CNRS, Rennes Métropole and Région Bretagne (AniDyn-MTgrant). DF's postdoctoral fellowship was funded by Région Bretagne (pRISM grant). HB's postdoctoral fellowship was funded by the European Molecular Biology Organization. TP was supported by the France-BioImaging infrastructure (ANR-10-INBS-04).

REFERENCES

Agresti, A. (2013). Categorical Data Analysis. Wiley.
Ahringer, J. (2003). Control of cell polarity and mitotic spindle positioning in animal cells. Current opinion in cell biology *15*, 73-81.
Barbosa, D.J., Duro, J., Prevo, B., Cheerambathur, D.K., Carvalho, A.X., and Gassmann, R. (2017). Dynactin binding to tyrosinated microtubules promotes centrosome centration in C. elegans by enhancing dynein-mediated organelle transport. PLoS Genetics *13*, e1006941.
Basset, A., Boulanger, J., Salamero, J., Bouthemy, P., and Kervrann, C. (2015). Adaptive spot detection with optimal scale selection in fluorescence microscopy images. IEEE Transactions on Image Processing *24*, 4512-4527.

Baumbach, J., Murthy, A., McClintock, M.A., Dix, C.I., Zalyte, R., Hoang, H.T., and Bullock, S.L. (2017). Lissencephaly-1 is a context-dependent regulator of the human dynein complex. eLife *6*, e21768.

Bellanger, J.-M., Carter, J.C., Phillips, J.B., Canard, C., Bowerman, B., and Gönczy, P. (2007). ZYG-9, TAC-1 and ZYG-8 together ensure correct microtubule function throughout the cell cycle of C. elegans embryos. Journal of Cell Science *120*, 2963-2973.

Bieling, P., Laan, L., Schek, H., Munteanu, E.L., Sandblad, L., Dogterom, M., Brunner, D., and Surrey, T. (2007). Reconstitution of a microtubule plus-end tracking system in vitro. Nature *450*, 1100-1105.

Bolker, B.M. (2008). Ecological Models and Data in R. Princeton University Press.

Boulanger, J.m., Kervrann, C., Bouthemy, P., Elbau, P., Sibarita, J.-B., and Salamero, J. (2010). Patch-based nonlocal functional for denoising fluorescence microscopy image sequences. Medical Imaging, IEEE Transactions on *29*, 442-454.

Bouvrais, H., Chesneau, L., Pastezeur, S., Fairbrass, D., Delattre, M., and Pécréaux, J. (2018). Microtubule Feedback and LET-99-Dependent Control of Pulling Forces Ensure Robust Spindle Position. Biophysical Journal.

Brenner, S. (1974). The genetics of Caenorhabditis elegans. Genetics *77*, 71-94.

Brouhard, G.J., Stear, J.H., Noetzel, T.L., Al-Bassam, J., Kinoshita, K., Harrison, S.C., Howard, J., and Hyman, A.A. (2008). XMAP215 Is a Processive Microtubule Polymerase. Cell *132*, 79-88.

Campbell, E.K.M., Werts, A.D., and Goldstein, B. (2009). A cell cycle timer for asymmetric spindle positioning. PLoS biology *7*, e1000088.

Chenouard, N., Smal, I., De Chaumont, F., Maška, M., Sbalzarini, I.F., Gong, Y., Cardinale, J., Carthel, C., Coraluppi, S., and Winter, M. (2014). Objective comparison of particle tracking methods. Nature methods *11*, 281-289.

Cockell, M.M., Baumer, K., and Gonczy, P. (2004). lis-1 is required for dynein-dependent cell division processes in C. elegans embryos. J Cell Sci *117*, 4571-4582.

Colin, A., Singaravelu, P., Théry, M., Blanchoin, L., and Gueroui, Z. (2018). Actin-Network Architecture Regulates Microtubule Dynamics. Current Biology *28*, 2647-2656.e2644.

Colombo, K., Grill, S.W., Kimple, R.J., Willard, F.S., Siderovski, D.P., and Gonczy, P. (2003). Translation of polarity cues into asymmetric spindle positioning in Caenorhabditis elegans embryos. Science *300*, 1957.

Costantino, S., Comeau, J.W., Kolin, D.L., and Wiseman, P.W. (2005). Accuracy and dynamic range of spatial image correlation and cross-correlation spectroscopy. Biophysical Journal *89*, 1251-1260.

Couwenbergs, C., Labbé, J.-C., Goulding, M., Marty, T., Bowerman, B., and Gotta, M. (2007). Heterotrimeric G protein signaling functions with dynein to promote spindle positioning in C. elegans. The Journal of Cell Biology *179*, 15-22.

D.L. Riddle, T.B., B.J. Meyer, J.R. Priess. (1997). C. elegans II.

DeSantis, M.E., Cianfrocco, M.A., Htet, Z.M., Tran, P.T., Reck-Peterson, S.L., and Leschziner, A.E. (2017). Lis1 Has Two Opposing Modes of Regulating Cytoplasmic Dynein. Cell *170*, 1197-1208 e1112.

Dogterom, M., Kerssemakers, J.W.J., Romet-Lemonne, G., and Janson, M.E. (2005). Force generation by dynamic microtubules. Current opinion in cell biology *17*, 67-74.

Duellberg, C., Cade, N.I., Holmes, D., and Surrey, T. (2016). The size of the EB cap determines instantaneous microtubule stability. eLife *5*, e13470.

Dujardin, D.L., and Vallee, R.B. (2002). Dynein at the cortex. Current opinion in cell biology *14*, 44-49.

Espiritu, E.B., Krueger, L.E., Ye, A., and Rose, L.S. (2012). CLASPs function redundantly to regulate astral microtubules in the C. elegans embryo. Dev Biol *368*, 242-254.
Faivre-Moskalenko, C., and Dogterom, M. (2002). Dynamics of microtubule asters in microfabricated chambers: the role of catastrophes. Proceedings of the National Academy of Sciences *99*, 16788-16793.
Fievet, B.T., Rodriguez, J., Naganathan, S., Lee, C., Zeiser, E., Ishidate, T., Shirayama, M., Grill, S., and Ahringer, J. (2013). Systematic genetic interaction screens uncover cell polarity regulators and functional redundancy. Nat Cell Biol *15*, 103-112.
Floyd, D., C Harrison, S., and van Oijen, A. (2010). Analysis of Kinetic Intermediates in Single-Particle Dwell-Time Distributions.
Fridolfsson, H.N., Ly, N., Meyerzon, M., and Starr, D.A. (2010). UNC-83 coordinates kinesin-1 and dynein activities at the nuclear envelope during nuclear migration. Dev Biol *338*, 237-250.
Garzon-Coral, C., Fantana, H.A., and Howard, J. (2016). A force-generating machinery maintains the spindle at the cell center during mitosis. Science *352*, 1124-1127.
Gerhold, A.R., Poupart, V., Labbé, J.-C., and Maddox, P.S. (2018). Spindle assembly checkpoint strength is linked to cell fate in the Caenorhabditis elegans embryo. Molecular Biology of the Cell *29*, 1435-1448.
Gigant, E., Stefanutti, M., Laband, K., Gluszek-Kustusz, A., Edwards, F., Lacroix, B., Maton, G., Canman, J.C., Welburn, J.P.I., and Dumont, J. (2017). Inhibition of ectopic microtubule assembly by the kinesin-13 KLP-7 prevents chromosome segregation and cytokinesis defects in oocytes. Development *144*, 1674-1686.
Gönczy, P. (2008). Mechanisms of asymmetric cell division: flies and worms pave the way. Nature Reviews Molecular Cell Biology *9*, 355-366.
Gonczy, P., Pichler, S., Kirkham, M., and Hyman, A.A. (1999). Cytoplasmic dynein is required for distinct aspects of MTOC positioning, including centrosome separation, in the one cell stage Caenorhabditis elegans embryo. Journal of Cell Biology *147*, 135-150.
Gotta, M., and Ahringer, J. (2001). Distinct roles for Galpha and Gbetagamma in regulating spindle position and orientation in Caenorhabditis elegans embryos. Nature cell biology *3*, 297-300.
Gotta, M., Dong, Y., Peterson, Y.K., Lanier, S.M., and Ahringer, J. (2003). Asymmetrically Distributed C. elegans Homologs of AGS3/PINS Control Spindle Position in the Early Embryo. Current Biology *13*, 1029-1037.
Goulding, M.B., Canman, J.C., Senning, E.N., Marcus, A.H., and Bowerman, B. (2007). Control of nuclear centration in the C. elegans zygote by receptor-independent Galpha signaling and myosin II. J Cell Biol *178*, 1177-1191.
Grill, S.W., GoÈnczy, P., Stelzer, E.H.K., and Hyman, A.A. (2001). Polarity controls forces governing asymmetric spindle positioning in theCaenorhabditis elegansembryo.
Grill, S.W., Howard, J., Schaffer, E., Stelzer, E.H.K., and Hyman, A.A. (2003). The distribution of active force generators controls mitotic spindle position. Science *301*, 518.
Grill, S.W., and Hyman, A.A. (2005). Spindle positioning by cortical pulling forces. Developmental Cell *8*, 461-465.
Grill, S.W., Kruse, K., and Julicher, F. (2005). Theory of mitotic spindle oscillations. Phys Rev Lett *94*, 108104.
Grinvald, A., and Steinberg, I.Z. (1974). On the analysis of fluorescence decay kinetics by the method of least-squares. Analytical Biochemistry *59*, 583-598.
Grishchuk, E.L., Molodtsov, M.I., Ataullakhanov, F.I., and McIntosh, J.R. (2005). Force production by disassembling microtubules. Nature *438*, 384.

Gusnowski, E.M., and Srayko, M. (2011). Visualization of dynein-dependent microtubule gliding at the cell cortex: implications for spindle positioning. Journal of Cell Biology *194*, 377-386.

Hendricks, Adam G., Lazarus, Jacob E., Perlson, E., Gardner, Melissa K., Odde, David J., Goldman, Yale E., and Holzbaur, Erika L.F. (2012). Dynein Tethers and Stabilizes Dynamic Microtubule Plus Ends. Current Biology *22*, 632-637.

Honda, Y., Tsuchiya, K., Sumiyoshi, E., Haruta, N., and Sugimoto, A. (2017). Tubulin isotype substitution revealed that isotype composition modulates microtubule dynamics in C. elegans embryos. J Cell Sci, jcs. 200923.

Howard, J. (2006). Elastic and damping forces generated by confined arrays of dynamic microtubules. Physical biology *3*, 54.

Jae Myung, I., Forster, M., and W. Browne, M. (2000). Special issue on model selection.

James, D.R., and Ware, W.R. (1985). A fallacy in the interpretation of fluorescence decay parameters. Chemical Physics Letters *120*, 455-459.

Janson, M.E., Mathilde, E., and Dogterom, M. (2003). Dynamic instability of microtubules is regulated by force. The Journal of cell biology *161*, 1029-1034.

Jaqaman, K., Loerke, D., Mettlen, M., Kuwata, H., Grinstein, S., Schmid, S.L., and Danuser, G. (2008). Robust single-particle tracking in live-cell time-lapse sequences. Nat Methods *5*, 695-702.

Jha, R., Roostalu, J., Cade, N.I., Trokter, M., and Surrey, T. (2017). Combinatorial regulation of the balance between dynein microtubule end accumulation and initiation of directed motility. The EMBO Journal *36*, 3387-3404.

Kalman, R.E. (1960). A new approach to linear filtering and prediction problems. Journal of basic Engineering *82*, 35-45.

Kamath, R.S., and Ahringer, J. (2003). Genome-wide RNAi screening in Caenorhabditis elegans. Methods *30*, 313-321.

Kimura, A., and Onami, S. (2005). Computer Simulations and Image Processing Reveal Length-Dependent Pulling Force as the Primary Mechanism for C. elegans Male Pronuclear Migration. Developmental Cell *8*, 765-775.

Kimura, A., and Onami, S. (2007). Local cortical pulling-force repression switches centrosomal centration and posterior displacement in C. elegans. The Journal of Cell Biology *179*, 1347-1354.

Kimura, K., and Kimura, A. (2011a). Intracellular organelles mediate cytoplasmic pulling force for centrosome centration in the Caenorhabditis elegans early embryo. Proceedings of the National Academy of Sciences *108*, 137-142.

Kimura, K., and Kimura, A. (2011b). A novel mechanism of microtubule length-dependent force to pull centrosomes toward the cell center. Bioarchitecture *1*, 74-79.

King, S.J., and Schroer, T.A. (2000). Dynactin increases the processivity of the cytoplasmic dynein motor. Nat Cell Biol *2*, 20-24.

Kozlowski, C., Srayko, M., and Nedelec, F. (2007). Cortical microtubule contacts position the spindle in C. elegans embryos. Cell *129*, 499-510.

Krueger, L.E., Wu, J.C., Tsou, M.F., and Rose, L.S. (2010). LET-99 inhibits lateral posterior pulling forces during asymmetric spindle elongation in C. elegans embryos. J Cell Biol *189*, 481-495.

Laan, L., Pavin, N., Husson, J., Romet-Lemonne, G., van Duijn, M., López, M.P., Vale, R.D., Jülicher, F., Reck-Peterson, S.L., and Dogterom, M. (2012a). Cortical Dynein Controls Microtubule Dynamics to Generate Pulling Forces that Position Microtubule Asters. Cell *148*, 502-514.

Laan, L., Roth, S., and Dogterom, M. (2012b). End-on microtubule-dynein interactions and pulling-based positioning of microtubule organizing centers. Cell Cycle *11*, 3750-3757.

Labbé, J.-C., McCarthy, E.K., and Goldstein, B. (2004). The forces that position a mitotic spindle asymmetrically are tethered until after the time of spindle assembly. The Journal of cell biology *167*, 245-256.
Labbé, J.C., Maddox, P.S., Salmon, E., and Goldstein, B. (2003). PAR Proteins Regulate Microtubule Dynamics at the Cell Cortex in C. elegans. Current Biology *13*, 707-714.
Labbe, J.C., McCarthy, E.K., and Goldstein, B. (2004). The forces that position a mitotic spindle asymmetrically are tethered until after the time of spindle assembly. J Cell Biol *167*, 245-256.
Laurence, T.A., and Chromy, B.A. (2010). Efficient maximum likelihood estimator fitting of histograms. Nature methods *7*, 338-339.
Lee, K.C.B., Siegel, J., Webb, S.E.D., Lévêque-Fort, S., Cole, M.J., Jones, R., Dowling, K., Lever, M.J., and French, P.M.W. (2001). Application of the Stretched Exponential Function to Fluorescence Lifetime Imaging. Biophysical Journal *81*, 1265-1274.
Li, S., Besson, S., Blackburn, C., Carroll, M., Ferguson, R.K., Flynn, H., Gillen, K., Leigh, R., Lindner, D., Linkert, M., Moore, W.J., Ramalingam, B., Rozbicki, E., Rustici, G., Tarkowska, A., Walczysko, P., Williams, E., Allan, C., Burel, J.-M., Moore, J., and Swedlow, J.R. (2016). Metadata management for high content screening in OMERO. Methods *96*, 27-32.
Maton, G., Edwards, F., Lacroix, B., Stefanutti, M., Laband, K., Lieury, T., Kim, T., Espeut, J., Canman, J.C., and Dumont, J. (2015). Kinetochore components are required for central spindle assembly. Nature cell biology *17*, 697-705.
Maus, M., Cotlet, M., Hofkens, J., Gensch, T., De Schryver, F.C., Schaffer, J., and Seidel, C.A.M. (2001). An Experimental Comparison of the Maximum Likelihood Estimation and Nonlinear Least-Squares Fluorescence Lifetime Analysis of Single Molecules. Analytical Chemistry *73*, 2078-2086.
McCarthy Campbell, E.K., Werts, A.D., and Goldstein, B. (2009). A cell cycle timer for asymmetric spindle positioning. PLoS Biol *7*, e1000088.
McNally, F.J. (2013). Mechanisms of spindle positioning. The Journal of cell biology *200*, 131-140.
Meiniel, W., Olivo-Marin, J.C., and Angelini, E.D. (2018). Denoising of Microscopy Images: A Review of the State-of-the-Art, and a New Sparsity-Based Method. IEEE Transactions on Image Processing *27*, 3842-3856.
Mitchison, T., and Kirschner, M. (1984). Dynamic instability of microtubule growth. Nature *312*, 237-242.
Morin, X., and Bellaïche, Y. (2011). Mitotic spindle orientation in asymmetric and symmetric cell divisions during animal development. Developmental cell *21*, 102-119.
Neumüller, R.A., and Knoblich, J.A. (2009). Dividing cellular asymmetry: asymmetric cell division and its implications for stem cells and cancer. Genes & development *23*, 2675-2699.
Nguyen-Ngoc, T., Afshar, K., and Gonczy, P. (2007). Coupling of cortical dynein and G[alpha] proteins mediates spindle positioning in Caenorhabditis elegans. Nat Cell Biol *9*, 1294-1302.
Nishimura, G., and Tamura, M. (2005). Artefacts in the analysis of temporal response functions measured by photon counting. Physics in Medicine and Biology *50*, 1327-1342.
O'Rourke, S.M., Christensen, S.N., and Bowerman, B. (2010). Caenorhabditis elegans EFA-6 limits microtubule growth at the cell cortex. Nat Cell Biol *12*, 1235-1241.
O'Rourke, S.M., Dorfman, M.D., Carter, J.C., and Bowerman, B. (2007). Dynein modifiers in C. elegans: light chains suppress conditional heavy chain mutants. PLoS Genet *3*, e128.

Oegema, K., Desai, A., Rybina, S., Kirkham, M., and Hyman, A.A. (2001). Functional analysis of kinetochore assembly in Caenorhabditis elegans. The Journal of Cell Biology *153*, 1209-1226.

Panbianco, C., Weinkove, D., Zanin, E., Jones, D., Divecha, N., Gotta, M., and Ahringer, J. (2008). A Casein Kinase 1 and PAR Proteins Regulate Asymmetry of a PIP2 Synthesis Enzyme for Asymmetric Spindle Positioning. Developmental Cell *15*, 198-208.

Park, D.H., and Rose, L.S. (2008). Dynamic localization of LIN-5 and GPR-1/2 to cortical force generation domains during spindle positioning. Developmental biology *315*, 42-54.

Pécréaux, J., Redemann, S., Alayan, Z., Mercat, B., Pastezeur, S., Garzon-Coral, C., Hyman, Anthony A., and Howard, J. (2016). The Mitotic Spindle in the One-Cell C. elegans Embryo Is Positioned with High Precision and Stability. Biophysical Journal *111*, 1773-1784.

Pecreaux, J., Röper, J.-C., Kruse, K., Jülicher, F., Hyman, A.A., Grill, S.W., and Howard, J. (2006a). Spindle Oscillations during Asymmetric Cell Division Require a Threshold Number of Active Cortical Force Generators. Current Biology *16*, 2111-2122.

Pecreaux, J., Zimmer, C., and Olivo-Marin, J.-C. (2006b). Biophysical active contours for cell tracking I: Tension and bending. Image Processing, 2006 IEEE International Conference on, 1949-1952.

Perlson, E., Hendricks, A.G., Lazarus, J.E., Ben-Yaakov, K., Gradus, T., Tokito, M., and Holzbaur, E.L.F. (2013). Dynein Interacts with the Neural Cell Adhesion Molecule (NCAM180) to Tether Dynamic Microtubules and Maintain Synaptic Density in Cortical Neurons. Journal of Biological Chemistry *288*, 27812-27824.

Praitis, V., Casey, E., Collar, D., and Austin, J. (2001). Creation of Low-Copy Integrated Transgenic Lines in Caenorhabditis elegans. Genetics *157*, 1217-1226.

Redemann, S., Pecreaux, J., Goehring, N.W., Khairy, K., Stelzer, E.H.K., Hyman, A.A., and Howard, J. (2010). Membrane invaginations reveal cortical sites that pull on mitotic spindles in one-cell C. elegans embryos. PloS one *5*, e12301.

Reid, D. (1979). An algorithm for tracking multiple targets. Automatic Control, IEEE Transactions on *24*, 843-854.

Reinsch, S., and Gonczy, P. (1998). Mechanisms of nuclear positioning. Journal of Cell Science *111*, 2283-2295.

Riche, S., Zouak, M., Argoul, F., Arneodo, A., Pecreaux, J., and Delattre, M. (2013). Evolutionary comparisons reveal a positional switch for spindle pole oscillations in Caenorhabditis embryos. The Journal of cell biology *201*, 653-662.

Rodriguez-Garcia, R., Chesneau, L., Pastezeur, S., Roul, J., Tramier, M., and Pécréaux, J. (2018). The polarity-induced force imbalance in Caenorhabditis elegans embryos is caused by asymmetric binding rates of dynein to the cortex. Molecular Biology of the Cell *29*, 3093-3104.

Sallé, J., Xie, J., Ershov, D., Lacassin, M., Dmitrieff, S., and Minc, N. (2018). Asymmetric division through a reduction of microtubule centering forces. The Journal of Cell Biology, jcb.201807102.

Schmidt, D.J., Rose, D.J., Saxton, W.M., and Strome, S. (2005). Functional analysis of cytoplasmic dynein heavy chain in Caenorhabditis elegans with fast-acting temperature-sensitive mutations. Mol Biol Cell *16*, 1200-1212.

Schwarz, G. (1978). Estimating the dimension of a model. The Annals of Statistics *6*, 461-464.

Severson, A.F., and Bowerman, B. (2003). Myosin and the PAR proteins polarize microfilament-dependent forces that shape and position mitotic spindles in Caenorhabditis elegans. J Cell Biol *161*, 21-26.

Shinar, T., Mana, M., Piano, F., and Shelley, M.J. (2011). A model of cytoplasmically driven microtubule-based motion in the single-celled Caenorhabditis elegans embryo. Proceedings of the National Academy of Sciences of the United States of America *108*, 10508-10513.

Siegel, J., Lee, K.B., Webb, S.E., Leveque-Fort, S., Cole, M.J., Jones, R., Dowling, K., French, P.M., and Lever, M. (2001). Application of the stretched exponential function to fluorescence lifetime imaging of biological tissue. European Conference on Biomedical Optics, 99-107.

Skop, A.R., and White, J.G. (1998). The dynactin complex is required for cleavage plane specification in early Caenorhabditis elegans embryos. Curr. Biol *8*, 1110-1116.

Splinter, D., Razafsky, D.S., Schlager, M.A., Serra-Marques, A., Grigoriev, I., Demmers, J., Keijzer, N., Jiang, K., Poser, I., Hyman, A.A., Hoogenraad, C.C., King, S.J., and Akhmanova, A. (2012). BICD2, dynactin, and LIS1 cooperate in regulating dynein recruitment to cellular structures. Mol Biol Cell *23*, 4226-4241.

Srayko, M., Kaya, A., Stamford, J., and Hyman, A.A. (2005). Identification and Characterization of Factors Required for Microtubule Growth and Nucleation in the Early C. elegans Embryo. Developmental Cell *9*, 223-236.

Srinivasan, D.G., Fisk, R.M., Xu, H., and Van Den Heuvel, S. (2003). A complex of LIN-5 and GPR proteins regulates G protein signaling and spindle function in C. elegans. Science's STKE *17*, 1225.

Sugioka, K., and Bowerman, B. (2018). Combinatorial Contact Cues Specify Cell Division Orientation by Directing Cortical Myosin Flows. Developmental Cell.

Sugioka, K., Fielmich, L.-E., Mizumoto, K., Bowerman, B., van den Heuvel, S., Kimura, A., and Sawa, H. (2018). Tumor suppressor APC is an attenuator of spindle-pulling forces during C. elegans asymmetric cell division. Proceedings of the National Academy of Sciences, 201712052.

Swan, A., Nguyen, T., and Suter, B. (1999). Drosophila Lissencephaly-1 functions with Bic-D and dynein in oocyte determination and nuclear positioning. Nat Cell Biol *1*, 444-449.

Tinevez, J.Y., J. Dragavon, L. Baba-Aissa, P. Roux, E. Perret, A. Canivet, V. Galy, and S. Shorte. (2012). A quantitative method for measuring phototoxicity of a live cell imaging microscope. Methods in Enzymology *506*, 291-309.

Tsou, M.-F.B., Hayashi, A., and Rose, L.S. (2003a). LET-99 opposes Gα/GPR signaling to generate asymmetry for spindle positioning in response to PAR and MES-1/SRC-1 signaling. Development *130*, 5717-5730.

Tsou, M.-F.B., Ku, W., Hayashi, A., and Rose, L.S. (2003b). PAR-dependent and geometry-dependent mechanisms of spindle positioning. The Journal of Cell Biology *160*, 845-855.

Turton, D.A., Reid, G.D., and Beddard, G.S. (2003). Accurate Analysis of Fluorescence Decays from Single Molecules in Photon Counting Experiments. Analytical Chemistry *75*, 4182-4187.

Urnavicius, L., Lau, C.K., Elshenawy, M.M., Morales-Rios, E., Motz, C., Yildiz, A., and Carter, A.P. (2018). Cryo-EM shows how dynactin recruits two dyneins for faster movement. Nature *554*, 202-206.

Vieland, V., and Hodge, S. (1998). Statistical Evidence: A Likelihood Paradigm.

Wright, A.J., and Hunter, C.P. (2003). Mutations in a β-tubulin disrupt spindle orientation and microtubule dynamics in the early Caenorhabditis elegans embryo. Molecular biology of the cell *14*, 4512-4525.

Wu, H.-Y., Nazockdast, E., Shelley, M.J., and Needleman, D.J. (2017). Forces positioning the mitotic spindle: Theories, and now experiments. BioEssays *39*, 1600212.

Wu, J.C., and Rose, L.S. (2007). PAR-3 and PAR-1 inhibit LET-99 localization to generate a cortical band important for spindle positioning in Caenorhabditis elegans embryos. Mol Biol Cell *18*, 4470-4482.

Wühr, M., Dumont, S., Groen, A.C., Needleman, D.J., and Mitchison, T.J. (2009). How does a millimeter-sized cell find its center? Cell Cycle *8*, 1115-1121.

Yogev, S., Maeder, C.I., Cooper, R., Horowitz, M., Hendricks, A.G., and Shen, K. (2017). Local inhibition of microtubule dynamics by dynein is required for neuronal cargo distribution. Nature Communications *8*, 15063.

Zanic, M., Stear, J.H., Hyman, A.A., and Howard, J. (2009). EB1 recognizes the nucleotide state of tubulin in the microtubule lattice. PLoS ONE *4*, e7585.

Zhu, J., Burakov, A., Rodionov, V., and Mogilner, A. (2010). Finding the Cell Center by a Balance of Dynein and Myosin Pulling and Microtubule Pushing: A Computational Study. Molecular Biology of the Cell *21*, 4418-4427.

MAIN FIGURES for the paper entitled "Two dynamical behaviours of the microtubules at cell cortex reveal pulling and pushing forces that position the spindle in *C. elegans* embryo."

14th May 2019

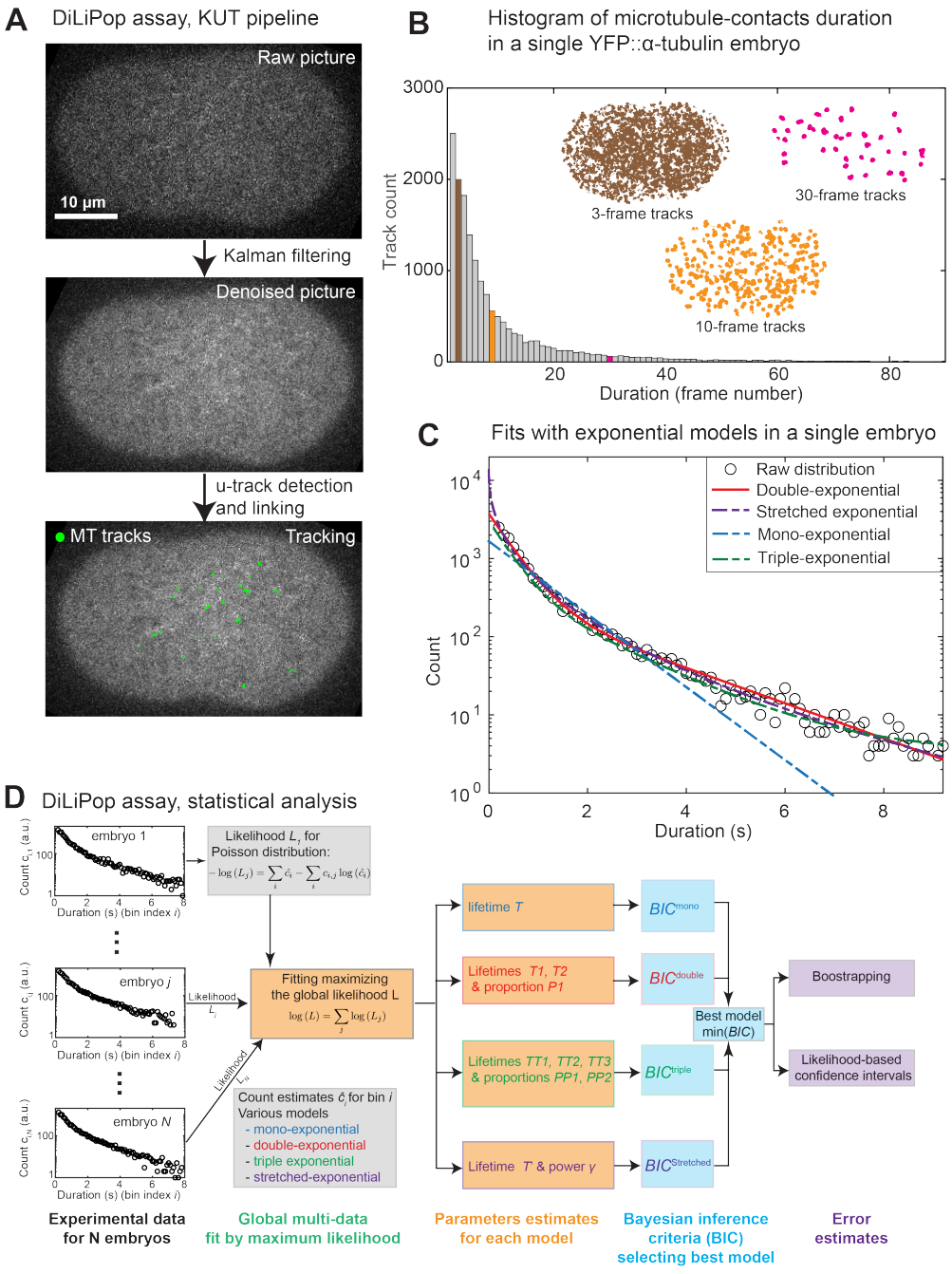

N = 25 untreated *C. elegans* embryos (α-tubulin::YPF labelling) - During metaphase and anaphase

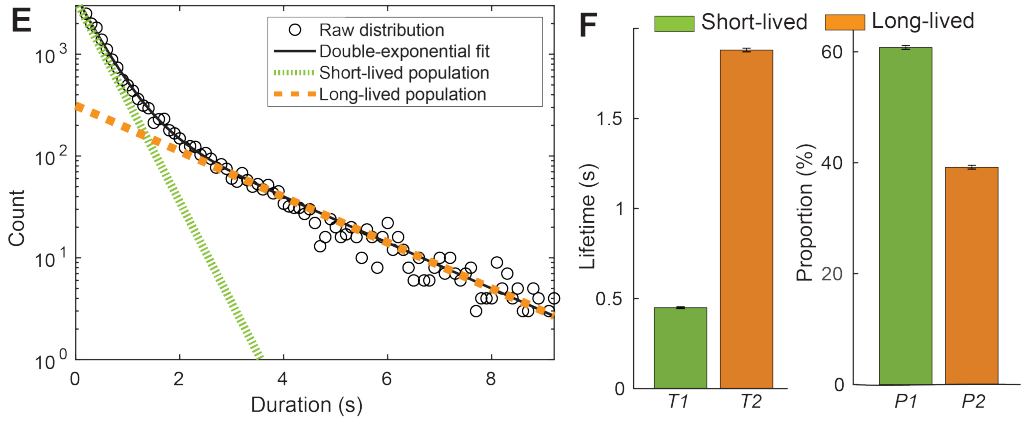

Figure 1: Microtubule dynamics at the cortex of the *C. elegans* embryo display two distinct behaviours during the first zygotic division.
(**A-D**) The typical workflow of the DiLiPop assay disentangles microtubule populations distinct by their dynamics (**A**) Exemplar KUT analysis of a one-cell embryo of *Caenorhabditis elegans* imaged at the cortex with the microtubules entirely labelled using YFP::α-tubulin. Their plus-ends appear as bright spots (top) (Movie S1), enhanced after denoising by a Kalman filter (middle). The trajectories of the microtubule contacts (green lines) are obtained using the u-track algorithm (bottom) (Supp. Text, §1.1.3). The analysis pipeline parameters are listed in Table S1. (**B**) Experimental distribution of the microtubule-contact durations for a typical untreated embryo imaged from nuclear envelope breakdown (NEBD) to late anaphase at 10 frames per second. (Insets) Spatial distributions of the contacts lasting 0.3 s (brown), 1 s (orange), and 3 s (pink). (**C**) The above experimental distribution (open circles) was fitted using various exponential models: mono-exponential (dashed blue line), double-exponential (plain red line), triple-exponential (dashed green line), and stretched exponential (dashed purple line) (Supp. Text, §1.2.1). (**D**) Schematic of the advanced statistical analysis in the DiLiPop assay (Supp. Text, §1.2). The experimental distributions of the microtubule-contact durations for N embryos (indexed by j) acquired in the same conditions were fitted using different exponential models and maximising the global maximum likelihood L, computed as the product of each embryo Poisson-distribution likelihood L_j (Supp. Text, §1.2.2). Exemplar distributions (histograms), depicting the count $c_{i,j}$ per bin indexed by i, are on the left part. The best model was selected as the one minimising the Bayesian Inference Criterion (*BIC*) (Supp. Text, §1.2.4). Finally, we estimated the standard errors on the best-model parameters by using either a Bootstrap approach or the likelihood-based confidence intervals (Supp. Text, §1.2.5). (**E**) The experimental distribution of microtubule-contact durations for the same set of $N = 25$ untreated embryos as in (D) and the global fit of each embryo by the best-fitting model, the double exponential (black line). The two separate contributions are highlighted: short-lived (dotted green line) and long-lived (dashed orange line). **(F)** Parameters obtained by fitting and corresponding error bars obtained by bootstrapping and their computation detailed in Supplemental Figure 1BC. The values of the Bayesian inference criteria (*BIC*) are reproduced in Table S2.

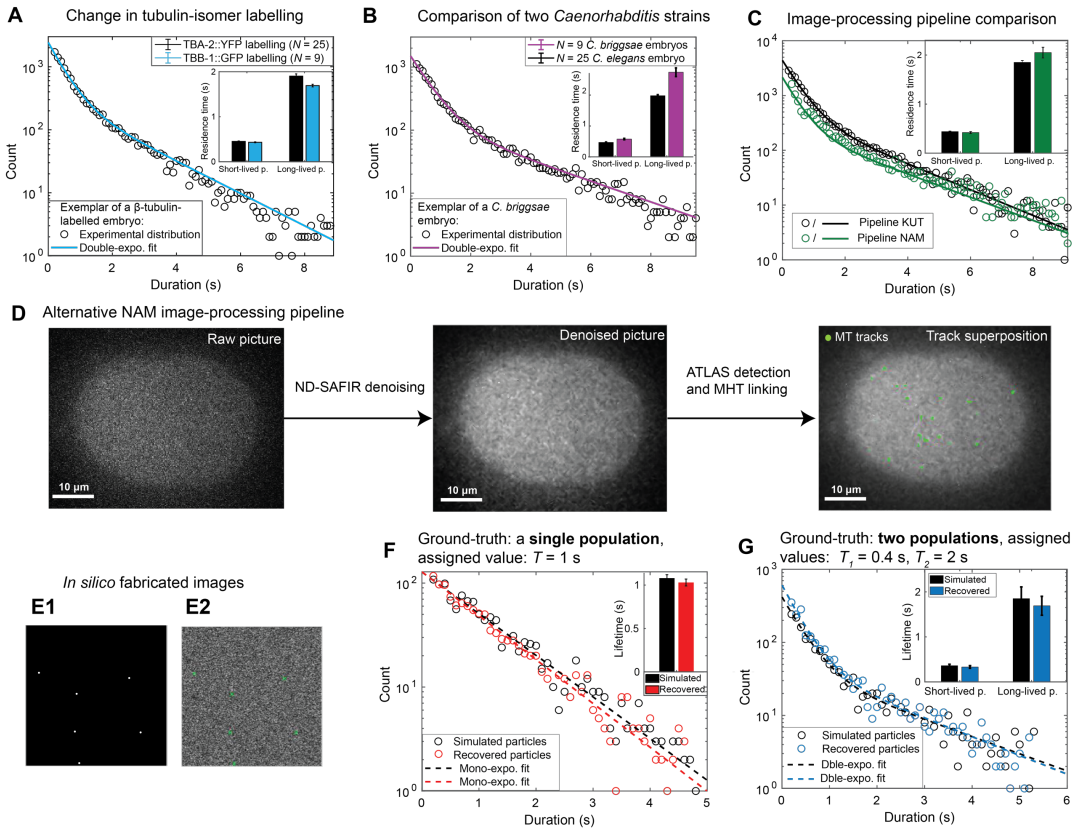

Figure 2: Validation of the two populations as being present at the cortex in tubulin-labelled embryo.

(**A**) Microtubule dynamics comparison during anaphase between α-tubulin labelled embryos (*N* = 25, black) and β-tubulin labelled embryos (*N* = 9, blue). Experimental distribution of the microtubule contact durations for a typical β-tubulin-labelled embryo fitted by a double exponential revealing the presence of two dynamical behaviours whose lifetimes are shown in inset. (**B**) Comparison of α-tubulin-labelled microtubule dynamics during anaphase between two different *Caenorhabditis* strains: *C. elegans* (*N* = 25 embryos, black, same data as ones displayed in the Figure 2A) and *C. briggsae* (*N* = 9, purple). Experimental microtubule-contact duration distribution for a typical *C. briggsae* embryo fitted by a double-exponential, whose lifetimes are shown in inset. In (A) and (B), to detect and link microtubule contacts, we used the KUT pipeline, whose parameter values are listed in Table S1. (**C**) Microtubule dynamics comparison when using two different image-processing pipelines for untreated α-tubulin-labelled embryos (*N* = 20): the pipeline KUT composed of the Kalman denoising and the u-track algorithm for spot-detecting and linking steps (parameter values listed in Table S1); the pipeline NAM composed of the ND-SAFIR denoising, the ATLAS spot-detecting and the MHT linking (parameter values displayed in Table S4) (Supp. Text §2.1.1). Experimental distributions of the microtubule-contact durations for a typical embryo using KUT pipeline (black) or NAM pipeline (green) for image processing. Using DiLiPop statistical analysis, both were best fitted by a double-exponential, whose lifetimes are displayed in inset. (**D**) Exemplar of a NAM analysis of a one-cell embryo of *C. elegans* imaged at the cortex with the microtubules entirely labelled using YFP::α-tubulin: raw image (left), ND-SAFIR denoised image (middle), and superposition of the trajectories of the microtubule contacts (green lines) obtained using the ATLAS detection and the MHT linker (right) (Supp. Text, §2.1.1). The analysis pipeline parameters are listed in Table S4. (**E-G**) Ground-truth validation of microtubule dynamics measures using *in silico* fabricated images. (E) The fabricated images were composed of particles (E1), which corresponded to the microtubule contacts, and of a background noise to mimic the *in vivo* one (E2). The particles tracked using the KUT pipeline are superposed and appear as green crosses. The parameters used for the generation of *in silico* images are listed in Table S3. (F) Simulation of particles with a single dynamical behaviour of lifetime equal to 1 s. The simulated-particle duration distribution (black

circles) and the recovered-track duration distribution (red circles) were both best fitted by a mono-exponential, each characterized by a lifetime shown in inset. (G) Simulation of two populations of particles characterized by lifetimes of 0.4 and 2 s. The simulated-particle duration distribution (black circles) and the recovered-track duration distribution (blue circles) were both best fitted by a double-exponential, whose lifetimes are shown in inset. In (F) and (G), we detected the particles using the KUT pipeline, whose parameter values are listed in Table S1.

A **Density maps of microtubule contacts after assignment** of each microtubule to either short- or long-lived population for *N* = 25 *C. elegans* untreated embryos (α-tubulin::YFP labelling).

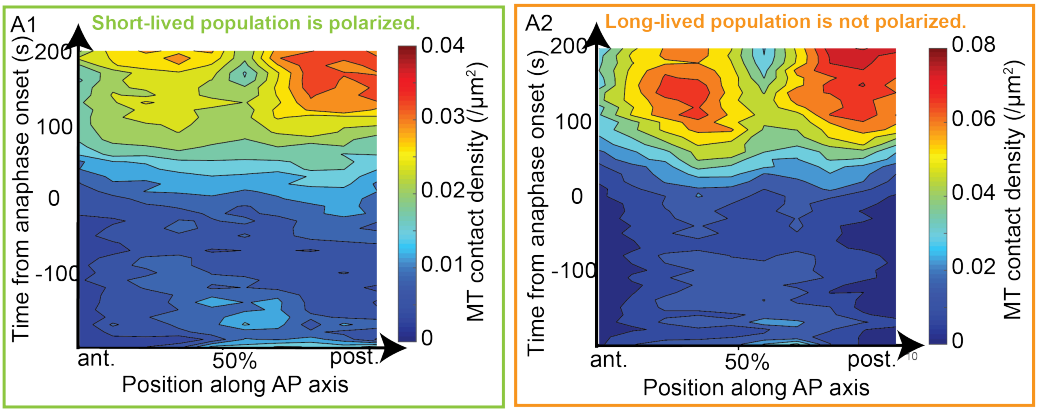

B **Density maps of microtubule contacts** assigned to the short-lived population after depleting GPR-1/2^{LGN} or CNSK-1.

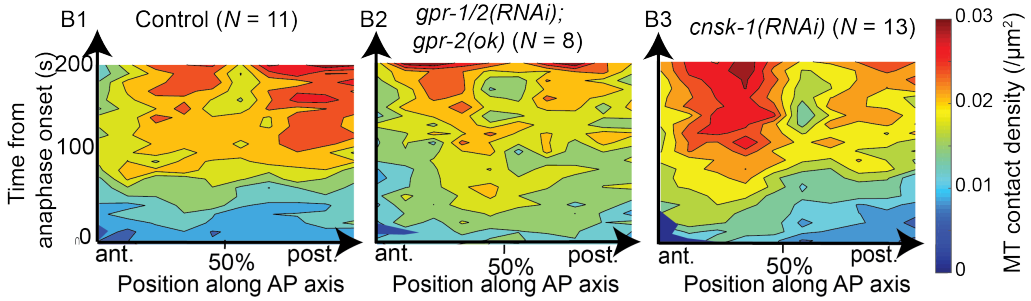

C **Lifetimes** of the short- and long-lived populations after depleting KLP-7^{MCAK} or ZYG-9$^{XMAP-215}$

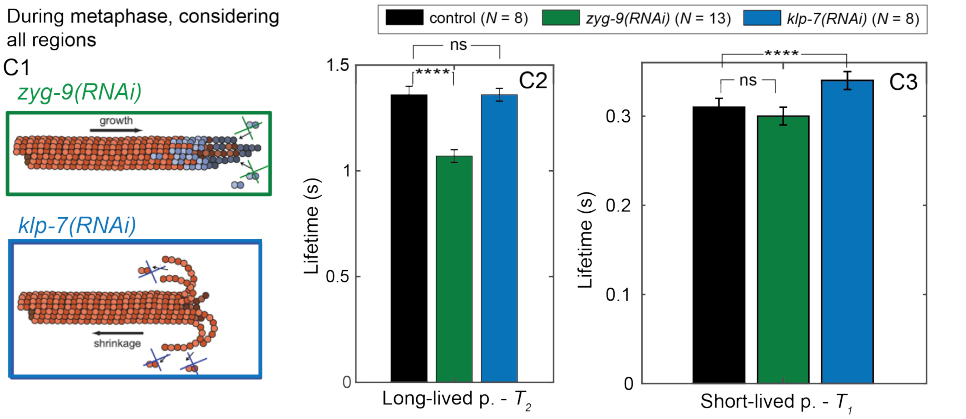

D **EB-labelling of the microtubules**

D1 EB-labelled-MT contact duration distribution

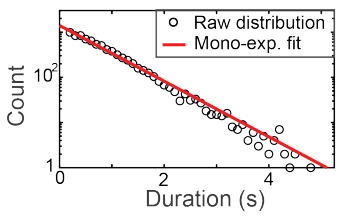

D2 Cortical lifetime: Tubulin- versus EB-labellings

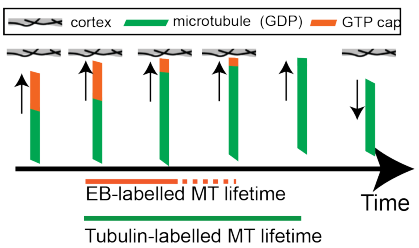

E Microtubules at the cortex involved in :

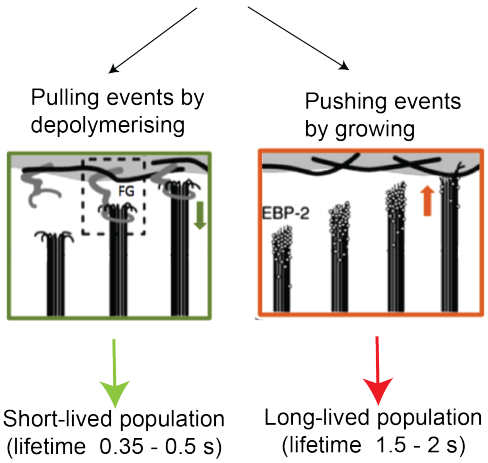

Figure 3: Microtubules pulling from and pushing against the cortex display short-lived and long-lived dynamical behaviours, respectively.

(**A**) Assignments of the microtubules to the short-lived or long-lived populations enabling to compute the DiLiPop density maps of microtubule contacts of the short-lived (A1) and long-lived (A2) populations for N = 25 untreated α-tubulin-labelled embryos. The densities, shown here as an interpolated heat map, were obtained by averaging the densities along the AP axis within 10 regions of equal width and over a 10 s running time window and finally taking the mean over embryos (Supp. Text, §1.3). (**B**) DiLiPop density maps of microtubule contacts assigned to the short-lived population to investigate the effects of GPR-1/2 or CNSK-1 depletions (Supp. Text, §1.3): (B1) for N = 11 control embryos, (B2) N = 8 *gpr-2(ok)gpr-1/2(RNAi)*-treated embryos and (B3) N = 13 *cnsk-1(RNAi)*-treated embryos. The associated density maps of microtubule contacts assigned to the long-lived population are displayed in Supplemental figure S4A. The local dynamical parameters of the two populations used for microtubule assignment to the short-lived population are displayed in Supplemental figure S4B1 and the centrosomal positions along mitosis of similarly treated embryos imaged at the spindle plane are shown in Supplemental figure S4C. (**C**) Microtubule dynamics at the cortex during metaphase when impairing either the growing rate through *zyg-9*$^{\text{XMAP-215}}$*(RNAi)* or the depolymerising rate through *klp-7*$^{\text{MCAK}}$*(RNAi)* (C1). Comparison of the lifetimes of the long-lived (C2) and short-lived (C3) populations in *zyg-9(RNAi)*-treated embryos (N = 13, green), *klp-7(RNAi)*-treated embryos (N = 8, blue) and control embryos (N = 8, black). Lifetime error bars are the standard deviations (SD) of the model-parameter distributions generated by bootstrapping (assuming Gaussian distribution) (Supp. Text, §1.2.5) and asterisks indicate significant differences. (**D**) Microtubule dynamics at the cortex of a EB-labelled stain (N = 9 embryos): (D1) Experimental microtubule-contact duration distribution during anaphase for a typical EB-labelled embryo, which was best fitted by a mono-exponential of lifetime equal to 0.64 ± 0.01 s. (D2) Schematic explaining the differences between the cortical residence time of the long-lived population of tubulin-labelled microtubules and the one of EB-labelled microtubules. (**E**) Two-population hypothesis: the short-lived microtubules are likely involved in pulling-force generating, while the long-lived microtubules include those growing against the cortex.

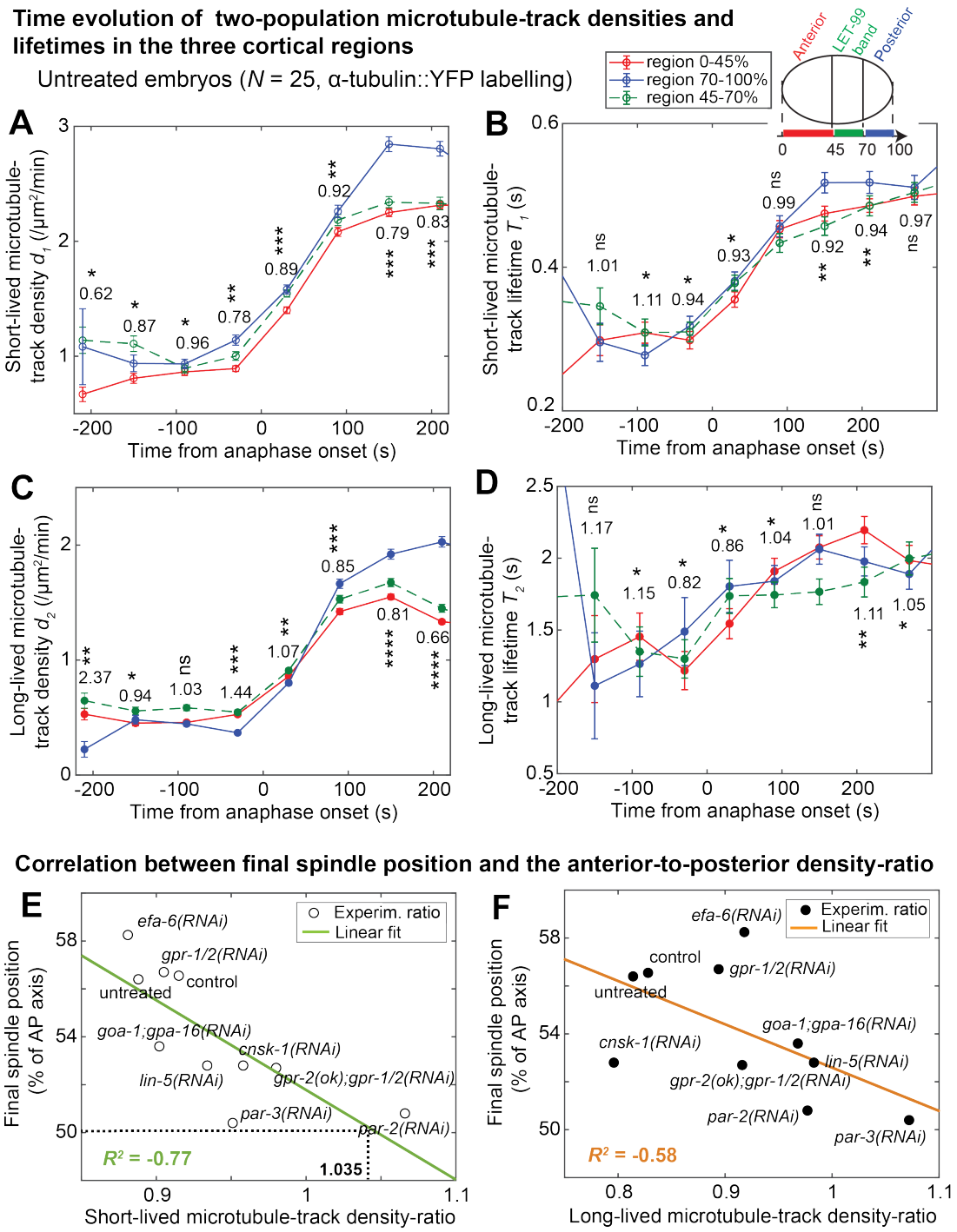

Figure 4: The polarised short-lived-population density, reflecting dynein on-rate, accounts for the pulling force imbalance and the final spindle-position.

(**A-D**) Temporal evolutions of the short-lived and long-lived population parameters: (A-B) density and lifetime of the short-lived population, (C-D) density and lifetime of the long-lived population, in the anterior region (red), lateral LET-99 band (green) and posterior-most crescent (blue), using 60 s time-windows, for untreated α-tubulin-labelled embryos (N = 25). The values indicated are the anterior (0-45% of AP axis) to posterior (70-100% of AP axis) ratio of either the densities (A&C) or the lifetimes (B&D). Asterisks indicate whether these two densities or lifetimes are significantly different. Associated errors of the model parameters were computed by the bootstrapping approach (Supp. Text, §1.2.5). (**E-F**) Plots of the final spindle position along the AP axis ($\mathcal{S}x$) versus the anterior (0-45% of AP axis) to posterior (70-100% of AP axis) density

ratio of the short-lived (E) and long-lived (F) populations during anaphase, with linear regressions shown in green and orange, respectively. Various depletions of proteins controlling the density of the pulling force generators and upstream polarity proteins were performed as two sets of similarly-treated experiments – firstly at the cortex to measure microtubule-contact densities, secondly at the spindle plane to track spindle poles: *par-3(RNAi)* (N = 10 at the cortex and N = 13 at the spindle plane, written as 10/13 for the following conditions), *par-2(RNAi)* (N = 9/16), *gpr-2(ok);gpr-1/2(RNAi)* (N = 8/8), *cnsk-1(RNAi)* (N = 13/10), *lin-5(RNAi)* (N = 13/14), *goa-1;gpa16(RNAi)* (N = 12/9), *gpr-1/2(RNAi)* (N = 11/6) and *efa-6(RNAi)* (N = 10/12), N = 11/10 control embryos and N = 25/9 untreated embryos.

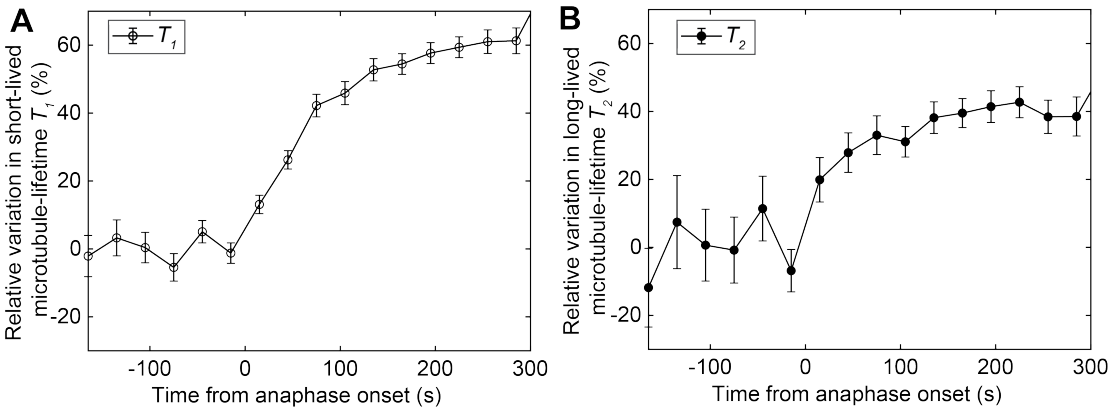

Figure 5: The short-lived-microtubule lifetime reflects the mitotic-progression control through the force generator processivity.

Temporal evolution of the microtubule-lifetime variations of the (A) short-lived and (B) long-lived populations in untreated α-tubulin-labelled embryos (N = 25), considering all cortical regions and using 30 s time-windows. Relative lifetimes are lifetimes normalized by the average of the metaphase raw lifetimes. Associated errors of the model parameters were computed by the bootstrapping approach (Supp. Text, §1.2.5).

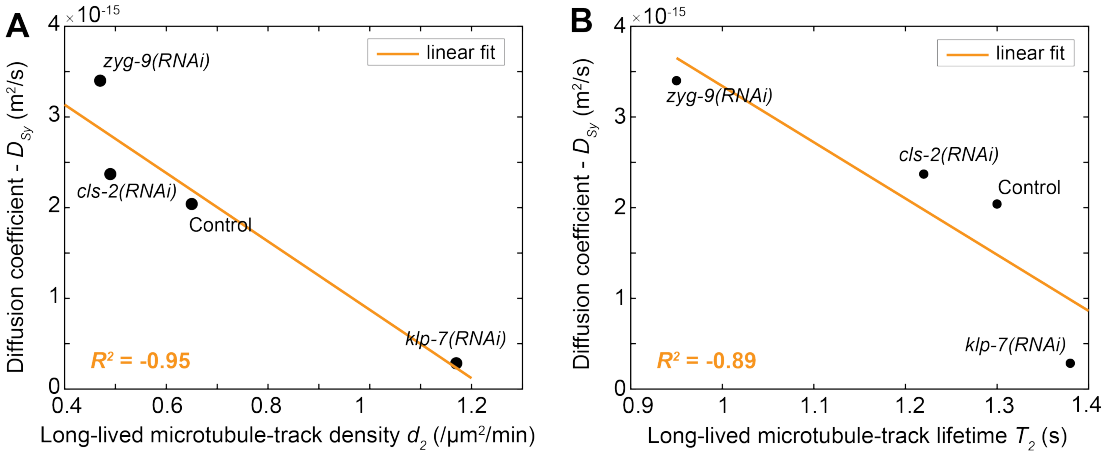

Figure 6: The polymerising microtubules create pushing forces involved in maintaining the spindle in cell centre.

Correlation between the diffusion coefficient of the spindle position along the transverse axis, D_{Sy}, and either (**A**) the microtubule-track density of the long-lived population, or (**B**) the microtubule-track lifetime of the long-lived population. Two sets of similarly-treated experiments – firstly at the cortex to measure microtubule dynamics, secondly at the spindle plane to track spindle poles: *klp-7(RNAi)* (N = 7 at the cortex and N = 12 at the spindle plane, written as 7/12 for the following conditions), *zyg-9(RNAi)* (N = 13/10), *cls-2(RNAi)* (N = 11/11) and control embryos (N = 8/13).

From microscopic-scale measures to cell-scale phenotypes

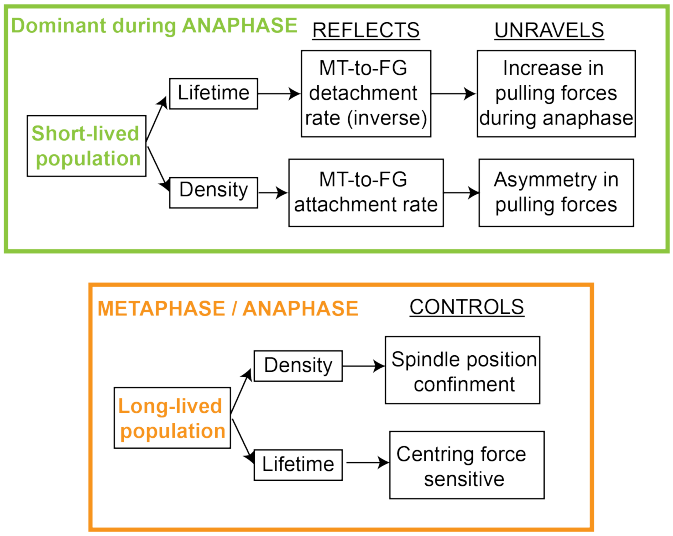

Figure 7: Schematic summarizing how microscopic-scale measurements of microtubule dynamics reflect cell-scale phenotypes of spindle positioning.